(p)ppGpp regulates a bacterial nucleosidase by an allosteric two-domain switch

Yong Zhang[a,1,*], René Lysdal Bærentsen[b,1], Tobias Fuhrer[c], Uwe Sauer[c], Kenn Gerdes[a], and Ditlev Egeskov Brodersen[b,2,*]

[a]*Centre of Excellence for Bacterial Stress Response and Persistence (BASP), Department of Biology, University of Copenhagen, DK-2200 Copenhagen, Denmark and* [b]*Department of Molecular Biology and Genetics, Aarhus University, DK-8000 Aarhus C, Denmark,* [c]*Institute of Molecular Systems Biology, Department of Biology, ETH, Zurich, Switzerland.*

[1] These authors contributed equally.

[2] Lead contact

* To whom correspondence should be addressed. Email addresses: Y.Z., yong.zhang@bio.ku.dk; D.E.B, deb@mbg.au.dk.

SUMMARY

The stringent response alarmones pppGpp and ppGpp are essential for rapid adaption of bacterial physiology to changes in the environment. In *Escherichia coli*, the nucleosidase PpnN (YgdH) regulates purine homeostasis by cleaving nucleoside monophosphates and specifically binds (p)ppGpp. Here, we show that (p)ppGpp stimulates the catalytic activity of PpnN both *in vitro* and *in vivo* causing accumulation of several types of nucleobases during stress. The structure of PpnN reveals a tetramer with allosteric (p)ppGpp binding sites located between subunits. pppGpp binding triggers a large conformational change that shifts the two terminal domains to expose the active site, providing a structural rationale for the stimulatory effect. We find that PpnN increases fitness and adjusts cellular tolerance to antibiotics and propose a model in which nucleotide levels can rapidly be adjusted during stress by simultaneous inhibition of biosynthesis and stimulation of degradation, thus achieving a balanced physiological response to constantly changing environments.

Keywords: YgdH, PpnN, allosteric enzyme, nucleotide metabolism, stringent response, antibiotic tolerance, persistence, fluoroquinolone

INTRODUCTION

Bacteria live in constantly changing environments and need to respond to a number of challenges, including limited nutrients and exposure to antibiotics. The stringent response, which involves a global reprogramming of cellular physiology during stress, is mediated by the two alarmone molecules, ppGpp (guanosine-5'-diphosphate-3'-diphosphate) and pppGpp (guanosine-5'-triphosphate-3'-diphosphate), which are 3' hyper-phosphorylated versions of GDP and GTP, respectively, and collectively referred to as (p)ppGpp (Cashel and Gallant, 1969). Production of (p)ppGpp has wide-ranging effects on bacterial physiology, including inhibition of ribosomal protein, rRNA and tRNA synthesis and stimulation of specific stress response genes (Traxler et al., 2008) Besides the well-characterised effects on transcription and translation, however, it is becoming increasingly evident that (p)ppGpp also affects many other cellular processes, including DNA replication and general metabolism (Hauryliuk et al., 2015; Liu et al., 2015a). (p)ppGpp is required for the virulence of pathogenic bacteria as well as multidrug tolerance via a physiological phenomenon known as *persistence*, so a deep understanding of the molecular mechanisms underlying the effects of (p)ppGpp on bacterial physiology is highly relevant for understanding human infectious diseases (Dalebroux et al., 2010; Harms et al., 2016).

Previously, we identified a number of (p)ppGpp binding and metabolising enzymes in *E. coli* K12 (Zhang et al., 2018). Among these, PpnN (YgdH) is unique in that (p)ppGpp binds to a site distinct from the catalytic pocket but the functional implications of this remained unclear. PpnN functions as a nucleosidase in purine nucleotide metabolism by cleaving nucleoside monophosphates to nucleobases and ribose-5'-phosphate (R5P) (Figures 1A and 1B). Interestingly, several other enzymes involved in purine nucleotide metabolism also bind (p)ppGpp (Hochstadt-Ozer and Cashel, 1972; Lopez et al., 1981; Pao and Dyess, 1981). These include inosine monophosphate (IMP)

dehydrogenase (GuaB) and adenylosuccinate synthetase (PurA), both required for *de novo* biosynthesis of GTP and ATP through conversion of IMP to xanthine monophosphate (XMP) and adenylosuccinate, respectively. Moreover, the three phosphoribosyl transferases Gpt, Hpt, and Apt required for the purine salvage biosynthesis pathway and thus responsible for recycling nucleobases to generate purine monophosphates, also bind (p)ppGpp. The enzymatic activity of all five proteins is consistently inhibited by (p)ppGpp. The scenario is thus that, during the stringent response, *E. coli* will consume ATP and either GTP or GDP to synthesize pppGpp and ppGpp, respectively, which in turn feedback inhibit further synthesis of purine nucleotides and hence (p)ppGpp as well (Figure 1A). In all these cases, (p)ppGpp functions as a competitive inhibitor by interfering the binding of IMP to GuaB and PurA, or the binding of 5'-phosphoribosyl 1'-pyrophosphate (PRPP) to Gpt and Hpt (Hochstadt-Ozer and Cashel, 1972; Lopez et al., 1981; Pao and Dyess, 1981; Zhang et al., 2018). In contrast, for PpnN, (p)ppGpp was shown to not compete with substrate binding, suggesting an allosteric mechanism of regulation (Zhang et al., 2018). Moreover, the nucleotide monophosphate cleavage activity of PpnN indicates that it functions in the opposite direction of the salvage biosynthesis enzymes, Gpt, Hpt, and Apt.

Here, we demonstrate that (p)ppGpp stimulates PpnN *in vitro* by an allosteric mechanism. Structural analysis reveals that (p)ppGpp binding induces a large conformational change of tetrameric PpnN that exposes the putative substrate binding pocket, thereby explaining the observed stimulation of PpnN activity. Analysis of intracellular metabolite concentrations confirms the role of PpnN in regulating purine metabolism *in vivo*, in particular accumulation of nucleobases during stress adaptation. We further show that PpnN and (p)ppGpp regulate the balance between competitive fitness and tolerance to antibiotics in *E. coli*. Finally, sequence comparison of PpnN orthologs among

Proteobacteria indicates that the (p)ppGpp-based activation mechanism is conserved in many important human pathogens.

RESULTS

Both pppGpp and ppGpp stimulate the catalytic activity of *E. coli* PpnN *in vitro*

We showed previously that *E. coli* PpnN binds both pppGpp and ppGpp at a site distinct from the substrate binding pocket, suggesting that the alarmone could act as an allosteric regulator (Zhang et al., 2018). To understand if (p)ppGpp affects the catalytic activity of PpnN, we purified His_6-PpnN to homogeneity (see STAR Methods for details) and used XMP (25 μM) as substrate, since XMP and its cleavage product, xanthine, exhibit significantly different extinction coefficients at 252 nm (Arent et al., 2006), and the reaction thus can be followed spectroscopically. Using this approach, we observed that both ppGpp and pppGpp (at 100 μM each) stimulated the activity of PpnN, with the pppGpp having the stronger effect (Figure S1A). To further support this, we used GMP as substrate and monitored the accumulation of the reaction product guanine by untargeted mass spectrometry (Figure 1B) (Fuhrer et al., 2011). Kinetic analysis both in the absence and presence of ppGpp and pppGpp showed that the *apo* enzyme displays a sigmoidal activity curve with GMP as substrate (Hill coefficient = 2.8 ± 0.2, EC50 = 414 ± 14 μM, Figure 1C), suggestive a cooperative binding of GMP to multiple active sites. The presence of pppGpp significantly boosted the catalytic activity at low GMP concentrations (< 250 μM) while maintaining a sigmoidal curve (Hill coefficient = 2.8 ± 0.6, EC50 = 62 ± 3 μM). In contrast, the presence of ppGpp showed Michaelis-Menten kinetics with a K_m value of 552 ± 19 μM (Hill coefficient = 1.2 ± 0.03). Notably, in the physiological range of GMP concentrations (~25 μM) (Bennett et al., 2009), both alarmones activate the enzyme significantly (Figures 1C and S1B). Taken together, these data conclusively demonstrate that PpnN is capable of

cleaving both GMP and XMP into nucleobase and R5P and is stimulated by both ppGpp and pppGpp in the physiological substrate range, with pppGpp having a more pronounced effect.

Stimulation of PpnN by (p)ppGpp causes accumulation of nucleobases *in vivo*

The observation that (p)ppGpp stimulates purified PpnN to degrade purine nucleotides *in vitro* complements previous studies showing that the alarmone inhibits the two *E. coli* phosphoribosyl transferases, Gpt and Hpt, in re-synthesizing the same nucleotides *in vivo* (Hochstadt-Ozer and Cashel, 1972). Together, these data support a dual role of (p)ppGpp in controlling intracellular purine nucleotide concentration during the stringent response (Figure 1A). The model predicts that when (p)ppGpp is produced, nucleobases will quickly accumulate due to the stimulated activity of PpnN and inhibited activities of Gpt/Hpt and consequently, deletion of *ppnN* should reduce this accumulation. To test this hypothesis, we exploited that production of (p)ppGpp and thus the stringent response can be induced in *E. coli* K-12 MG1655 by addition of valine in MOPS minimal medium, as this causes isoleucine starvation (Leavitt and Umbarger, 1962) (see STAR Methods for details). Both *E. coli wt* and a Δ*ppnN* in-frame deletion mutant strain were grown to early exponential phase (OD_{600} ~0.1) and valine was added to induce rapid physiological adaptation, as demonstrated by the presence of a new steady state growth curve with shallower slope (Figure S1C). Samples were taken via fast filtration just before and at several time points after addition of valine, and nucleotide pools extracted and analysed by untargeted mass spectrometry as previously reported (Link et al., 2013). Using this approach, we observed a sudden and significant increase in the levels of the nucleobases guanine, xanthine, and hypoxanthine in *wt* cells at 5 min post induction of starvation, quickly declining to basal levels (Figures 1D and S1D). Thymine and cytosine displayed similar trends but of lower magnitude (Figure S1E) while adenine could not be identified due to mass overlap with 2-hydroxymethylserine. We also observed increased levels of two other degradation products of purine

nucleobases, urate and allantoin, in the *wt* strain (Figure S1F). The decline in nucleobase concentration from 5-10 min could thus be a result of further degradation and excretion as reported before (Link et al., 2015; Rinas et al., 1995), or re-use to support growth, or both. Importantly, neither the sudden increase nor the subsequent decline were observed in the Δ*ppnN* strain, suggesting that PpnN is directly responsible for accumulation of the nucleobases. To exclude the possibility that changes in PpnN expression levels could be a contributing cause, we confirmed that protein levels were constant in the *wt* strain throughout the experiment (Figure S1G). Moreover, we used autoradiography to confirm that both pppGpp and ppGpp are rapidly produced as early as two minutes after addition of valine in both the Δ*ppnN* mutant and *wt* strains, consistent with induction of the stringent response (Figure S1H). Taken together, our observations are thus consistent with a model in which starvation of *E. coli* causes production of (p)ppGpp, which in turn activates constitutively expressed PpnN to degrade primarily purine nucleotides to free nucleobases.

PpnN forms a tetramer via two domains of unknown function (DUFs) flanking a core catalytic domain

To understand the molecular and mechanistic basis for regulation of *E. coli* PpnN by (p)ppGpp, we determined the crystal structure of the enzyme in its *apo* form to 2.5 Å by molecular replacement using an unpublished and uncharacterised structure of an ortholog from *Vibrio cholerae* as search model (PDB ID 2PMB) (Bonanno et al., 2005). The asymmetric unit contains two protein chains that are complete except for the last 14-15 residues and the flexible loop 112-122 (Figure S2). The final structure has R_{work}/R_{free} values of 21.2%/26.9% with good overall statistics for the resolution range (see Table 1 for crystallographic statistics). *E. coli* PpnN consists of three distinct domains, an N-terminal domain (residues 1-149), a central catalytic domain (residues 150-331), and a C-terminal domain (residues 332-454) (Figures 2A and S2). Both the N and C-terminal domains are

uncharacterised folds (DUF4478/PF14793 and DUF3412/PF11892, respectively) but we note that they are often found together, flanking a core Rossmann fold domain (PF03641, LOG family, InterPro IPR031100). The N-terminal domain is composed of a three-stranded anti-parallel β-sheet surrounded by α-helices, most of which form the main interface to the central domain (Figures 2A and S3A). The last part of the domain including α6, extends away from the core fold and wraps around the central domain. The central, catalytic domain has a classical Rossmann-like fold consisting of a seven-stranded parallel β-sheet and surrounding α-helices (Figures 2A and S3A) (Rao and Rossmann 1973). Finally, the smaller C-terminal domain is completely α-helical and also has an extension that wraps around the central domain (Figure S3A).

Analysis of protein interfaces using PISA (Krissinel and Henrick, 2007) reveals that PpnN likely forms a tetramer, an observation which was confirmed in solution by size exclusion chromatography (see below). In the crystals of the *apo* form, the dimer interface is quite loose and primarily maintained by reciprocal interactions of loop regions in the N and C terminal domains (residues 67-72 and 343-348, Figure 2B, circles) while the molecules pack more closely along a separate, extensive interaction interface to form the complete tetramer (Figure 2B). The overall structure is similar to two structures of uncharacterised proteins from *Vibrio cholerae* (PDB IDs 2PMB, 3GH1, 4NPA) and *Idomarina baltica*, (PDB ID 3BQ9) with root mean square deviations (rmsds) between Cα atoms of 0.99 (PpnN to 2PMB) and 1.69 Å (PpnN to 3BQ9), respectively (Figure S3B) (Baugh et al., 2015; Bonanno et al., 2005). The presence of a well-known nucleotide-binding fold as well as a highly conserved PGGxGTxxE motif (residues 256-264, Figure S2), found in other enzymes with nucleosidase-like activities allows us to predict the location of the putative active site near the C-terminal end of β4 and β5 with high certainty (Figure 2A) (Dzurova et al., 2015). Despite the conserved nature of the motif, however, the precise involvement of the individual residues in substrate binding and catalysis are not

known. Alignment with the structure of an uncharacterised nucleotide-binding protein from *Mycobacterium marinum* showing similarity to the PpnN core domain and determined in the presence of adenosine monophosphate (AMP) (PDB ID 3SBX, Figure S3C) (Baugh et al., 2015), however, suggests that H157, R241, T261, and E264 of PpnN are likely to be involved in either substrate binding and/or catalysis (Figures S3D and S3E). Finally, we note that of these, His157 was found to coordinate a phosphate or sulphate ion in both of the two homologous structures from *Vibrio cholerae* and *Idomarina baltica*, at a similar position to the phosphate of AMP in the *M. marinum* structure, suggesting that these ions mimic a phosphate group. In summary, structural analysis reveals that *E. coli* PpnN consists of a core Rossmann-like catalytic domain with a conserved active site and N and C terminal DUF domains required for the tetrameric state of the enzyme.

The (p)ppGpp binding site is located between the N and C terminal DUF domains

To understand how the presence of alarmone can affect the activity of PpnN, we incubated the enzyme with 1 mM pppGpp prior to crystallisation and determined the structure to 2.8 Å using the *apo* structure as search model. The resulting model was refined to final R_{work}/R_{free} = 18.1%/23.2% with good overall statistics (see Table 1 for details). The pppGpp-bound structure is complete for residues 1-438 (out of 459 in total) and thus includes the flexible loop regions missing in the *apo* structure. Inspection of the initial, unbiased mF_o-DF_c difference electron density map reveals the presence of a single pppGpp binding site per monomer, located at the dimer interface observed in the *apo* form (Figure 2B and S4A). There is thus a total of four active sites and four (p)ppGpp binding sites per tetramer. The pppGpp binding pocket is formed between adjacent molecules with the 5'-phosphate groups in close proximity to R68, R70, and K73 of the N-terminal domain of one monomer and the 3'-phosphate groups pointing towards R341 and K337 from the C-terminal domain of a nearby monomer (Figures 2C, 2D, 2E, and S2). The two sets of basic residues are thus located on the N and

198 C terminal DUF domains and highly conserved among PpnN orthologs in Proteobacteria (Figures 2F
199 and S4B). Recognition of the guanine nucleobase is accomplished partly by sandwiching between
200 Y347 and R70 and partly through specific interactions between the exocyclic amino group (N2) and
201 the main chain carbonyl atom of D345 as well as between the guanine O6 carbonyl group and the
202 main chain amino group of Y347 (Figures 2C, 2D, and S2). In summary, we find that pppGpp binds
203 between the N and C terminal DUF domains of PpnN monomers and is thus dependent on the
204 tetrameric state of the enzyme.
205
206 **Binding of pppGpp activates PpnN by exposing the catalytic pocket**
207 In the *apo* form, the pppGpp binding pocket is closed by inter-domain interactions formed between
208 R70 and the main chain carbonyl groups of residues 145-146 of the adjacent monomer as well the
209 conserved E69 that appears to counter the positive residues in the region (Figure 2C). Upon binding
210 of pppGpp, these interactions are broken and the binding pocket opens to accommodate the ligand,
211 which causes the loop 68-70 to shift back and above the 342-345 region, while E69 moves away and
212 points in the opposite direction compared to the *apo* form, away from the binding site (Figure 2D).
213 Comparison of the overall conformations of the *apo* and pppGpp-bound PpnN monomers reveals that
214 these subtle changes result in large-scale rearrangements involving movements of the entire N and
215 C-terminal DUF domains relative to the central catalytic domain (Figure 3A and Movie S1). In the
216 *apo* form, access to the putative active site is relatively restricted due to interactions between the
217 loops 49-51 ("50 loop", N-terminal domain) and 399-402 ("400 loop", C-terminal domain). Despite
218 interacting, these loops have relatively poor electron density in the *apo* form, suggesting that they are
219 flexible and probably allows some degree of access of substrate to the active site. Such flexibility
220 could thus explain the basal activity of PpnN observed in the absence of (p)ppGpp (Sevin et al., 2017).
221 On the contrary, in the pppGpp-bound form, the two loops have moved far apart (~20 Å) causing the

putative active site to become widely solvent exposed (Figure 3A). The mechanical force required for this movement appears to come directly from simultaneous interactions with pppGpp at both the N and C-terminal DUF domains and to be mediated by the domain extensions that connect to the catalytic domain (Figure S3A). Given that the two DUF domains also mediate tetramer formation (Figure 2C, see below), it is natural to assume that they also impose some level of cooperativity with respect to either ligand or substrate binding, or both, consistent with the observed allosteric kinetics. In summary, binding of pppGpp to *E. coli* PpnN induces a large-scale rearrangement of the two DUF domains opening up the active site. We believe that the increased accessibility of the active site is likely the main reason for the observed stimulatory effect on PpnN activity upon binding (p)ppGpp.

Mutations abolishing (p)ppGpp binding reduce the stimulation of enzymatic activity

To probe the importance of the residues directly involved in coordinating pppGpp (R68, R70, K73, R341 and Y347), residues were mutated to alanine both individually and in combinations corresponding to whether they primarily interact with the 5' (R68A/R70A/K73A, "RRK") or 3' (R341A/Y347A, "RY") phosphate groups of the ligand. All mutant proteins were each expressed, purified to homogeneity (Figure S4C) and analysed by size-exclusion chromatography (Figure S4D). Most mutants (R68A, R70A, K73A, R341A, and RRK) showed elution profiles very similar to that of the wild type, indicating only minor structural changes. However, two mutants, Y347A and RY, eluted significantly later during gel filtration suggesting that the tetrameric state is disrupted. In the *apo* structure, Y347 is located on the surface of the C-terminal domain directly facing the loop 68-73 in the N-terminal domain of an adjacent PpnN monomer (Figures 2C and 3B) suggesting that it could be involved in multimerisation in the *apo* state as well as pppGpp binding. Consistently, the RY double mutation also failed to form a tetramer (Figure S4D).

We next determined binding affinities of the mutant proteins towards pppGpp by the DRaCALA method using radiolabelled α-^{32}P-pppGpp (Orr and Lee, 2017; Zhang et al., 2018). As expected, the mutants showed deficiency in binding pppGpp to various extents, with the double RY and triple RRK mutants as well as Y347A having the lowest affinities (Figure 3C). Of these, RY and Y347A that do not form a tetramer likely cannot bind pppGpp at all. Moreover, the binding assay also confirmed the importance of the RRK motif in binding pppGpp, despite this mutant maintaining the tetramer form. Very similar binding curves of the mutant proteins were observed for α-^{32}P-ppGpp (Figure S4E), strongly suggesting that the two alarmone molecules bind to the same site. Quantification shows that wild type PpnN has a slightly higher affinity for pppGpp (K_d = 3.4 ± 0.3 μM, Figure 3C) than ppGpp (K_d = 6.6 ± 2.4 μM, Figure S4E), consistent with previous studies (Zhang et al., 2018), the higher stimulatory potency of pppGpp, and the PpnN structure. To test if the reduced binding affinity of the mutants towards pppGpp and ppGpp is also associated with a lower level of stimulation of enzymatic activity as would be expected, we repeated the XMP assay for the double (RY) and triple (RRK) mutants and found that both mutants displayed significantly reduced responses to pppGpp (Figure 3D, dark bars). Surprisingly, the basal activities of both mutant PpnN proteins were higher than that of *wt* PpnN in the absence of (p)ppGpp (Figure 3D, grey bars), which suggests that the overall tetrameric conformation serves to constrain relatively high basal activity of the monomeric/dimeric enzyme. This is consistent with the observation that key residues involved in (p)ppGpp binding are also important for tetramer formation and that mutation of these residues leads to both reduced binding of (p)ppGpp and increased basal enzymatic activity.

PpnN affects *E. coli* fitness and antibiotic tolerance

Nucleobases are energetically expensive to synthesize *de novo* and are therefore thought to fuel fast regrowth of bacterial cells after dormancy by entering directly into the salvage biosynthesis pathways

(Link et al., 2015). Consistent with its role in purine metabolism, PpnN was previously found to promote regrowth of glucose-starved *E. coli* cells from stationary phase (Sevin et al., 2017). Bacteria such as *E. coli* live naturally in environments characterised by frequent feast-or-famine cycles. To mimic this experimentally and test the potential involvement of PpnN, a co-growth scheme was designed in which stationary phase cells of *wt* and Δ*ppnN* mutant strains were mixed in an equal ratio, then sub-cultured in fresh media and allowed to reach stationary phase, after which they again were diluted and regrown in fresh medium ("Log-Stat", Figure S5A). As a control, a feast-only scheme ("Log", Figure S5B) was also designed, where mixed cells of both strains were kept constantly in fresh medium. To follow the fraction of Δ*ppnN* cells in the mixed population over time, we replaced the *lacZ* allele of *wt E. coli* by a kanamycin resistance cassette (*wt lacZ::kan*) allowing visual determination of the number of cells of a given type on X-gal plates (see STAR Methods for details). Using this approach, we found that the fraction of Δ*ppnN* in the population stayed relatively constant over ~30 generations under the Log scheme, indicating the dispensability of *ppnN* for cell fitness under this condition (Figure 4A). In contrast, the fraction of Δ*ppnN* cells dropped to ~20% after co-culturing under the Log-Stat scheme, suggesting a significant fitness defect in Δ*ppnN* during feast-and-famine cycles (Figure 4A). As a control for the effect of the *lacZ* gene replacement, we repeated the experiment in a setting where the *wt* strain was co-cultured with a Δ*ppnN lacZ::kan* strain and obtained similar results (data not shown). Together, these data suggest that *ppnN* positively affects fitness under nutrient fluctuating conditions, potentially by breaking down nucleotides into nucleobases during starvation that can support efficient regrowth when nutrients become available again.

Both a slow growth rate and a long lag phase have been shown to contribute to persistence in *E. coli* (Balaban et al., 2004; Fridman et al., 2014; Tuomanen et al., 1986). Given the importance of *ppnN* in

competitive fitness, we therefore tested the tolerance of *E. coli wt* and the Δ*ppnN* strain towards multiple antibiotics, namely ampicillin (targeting the cell wall), gentamicin (targeting the small ribosomal subunit), and the fluoroquinolone antibiotics, ofloxacin and ciprofloxacin (both targeting DNA gyrase and topoisomerase IV). In each case, we measured persister cell levels over time upon growth resumption after 16 h overnight stationary growth (Figure S5C). Highly reproducible persister levels were observed for both ofloxacin (Figure 4B) and ciprofloxacin (Figure S5D), but neither ampicillin nor gentamicin (data not shown). Persister levels for both the *wt*, Δ*ppnN* and the complementation strain Δ*ppnN:ppnN*$_{wt}$ were found to drop from the beginning of regrowth to mid-log phase (0-2 h, "phase I") and to increase thereafter during the transition to stationary phase (2-5 h, "phase II", Figure 4B). This is consistent with ofloxacin and ciprofloxacin killing off actively growing cells and that regrowth involves resuscitation of quiescent stationary phase cells. Importantly, the Δ*ppnN* strain produced ~10 times more persisters than *wt* during phase I, while similar levels of persisters were produced by both strains in phase II. The difference could be complemented *in situ* by the *wt ppnN* allele (Figure 4B) and the same trend was observed for ciprofloxacin-tolerant persister cells of the three strains (Figure S5D). We conclude that the decreased competitive fitness of the Δ*ppnN* strain likely accounts for the increased number of persister cells, either due to introduction of a slightly longer lag phase or slower overall growth rate (Balaban et al., 2004; Fridman et al., 2014; Tuomanen et al., 1986).

(p)ppGpp fine-tunes the physiological function of PpnN

Finally, we asked if (p)ppGpp controls the *ppnN*-dependent effects on cell fitness and persistence by *in situ* complementation using either the *ppnN*$_{RRK}$ or *ppnN*$_{RY}$ alleles that encode mutant PpnN proteins deficient in (p)ppGpp binding. In contrast to Δ*ppnN*, both Δ*ppnN::ppnN*$_{RRK}$ and Δ*ppnN::ppnN*$_{RY}$ were observed to outperform the *wt lacZ::kan* strain after ~30 generations in the Log-Stat co-growth

assay, while Δ*ppnN::ppnN*$_{wt}$ displays similar fitness to *wt lacZ::kan* under the same conditions (Figure 4C). Western blots confirmed that both variants were expressed at similar levels to *wt* PpnN (Figure S5E) during regrowth, arguing that the increased competitive fitness can be attributed to the higher basal enzymatic activities of both PpnN$_{RRK}$ and PpnN$_{RY}$. Consistently, both Δ*ppnN::ppnN*$_{RRK}$ and Δ*ppnN::ppnN*$_{RY}$ were found to produce significantly more colony forming units (CFUs) than the *wt* strain during regrowth (Figure 4D, 2 h time point). The faster regrowth and increased fitness of Δ*ppnN::ppnN*$_{RRK}$ and Δ*ppnN::ppnN*$_{RY}$ should make these strains more susceptible to ofloxacin. Indeed, we find that both mutant strains produce significantly fewer persisters than Δ*ppnN::ppnN*$_{wt}$ or a *wt* strain during phase I (Figure 4D). Our data thus support a model wherein (p)ppGpp is able to fine-tune the activity of PpnN to regulate purine metabolism, resulting in an optimised balance of cell proliferation and antibiotic tolerance under stressful conditions.

DISCUSSION

Regulation of PpnN by (p)ppGpp is conserved among Proteobacteria

In this study, we found that (p)ppGpp allosterically stimulates the activity of PpnN. This mechanism is reminiscent of the *E. coli* lysine decarboxylase LdcI and RNA polymerase, to which ppGpp also binds as an allosteric regulator (Kanjee et al., 2011; Ross et al., 2016). Interestingly, the number of positively charged residues in PpnN coordinating the 5' and 3' phosphate groups of pppGpp precisely matches the number of phosphate groups on either side of the molecule (Figure 2E). Mutation of a single of the 5'-interacting residues (R70 and R68) about halves the fraction of bound (p)ppGpp and it thus appears unlikely that it is simply the presence of three positive charges at this site that confers a preference for pppGpp over ppGpp. It is more likely that the two groups of positive residues serve to select against GTP, which has no 3' phosphate groups. Structurally, PpnN can accommodate GTP at the allosteric site, but we speculate that only pppGpp and ppGpp have a conformation favourable

for binding to the protein. It has recently been shown that (p)ppGpp displays a number of unique conformations of its two phosphate tails that are unlike those observed for GTP (Steinchen and Bange, 2016). This view is supported by the PpnN$_{RRK}$ triple mutant, in which all 5' phosphate-interacting residues have been removed and we observe an almost complete loss of alarmone binding (Figure 3C and S4E), suggesting that interactions with the 3' phosphate groups of (p)ppGpp alone are not sufficient to support binding. The PpnN$_{RY}$ variant does not exist on the tetrameric form, which suggests that the (p)ppGpp-binding site not only serves to bind the alarmone, but also stabilises oligomerisation. Interestingly, this mutant exhibits an increased enzymatic activity compared to *wt* PpnN, suggesting that the monomer is more active and consequently that tetramer formation serves to limit this basal activity as seen for other allosteric enzymes involved in nucleotide biosynthesis, such as aspartyl transcarbamoylase (ATCase) (Gerhart and Schachman, 1965).

Analysis of the sequences of 668 PpnN orthologs (see STAR Methods for details) reveals that PpnN-like proteins are widespread among β- and γ-Proteobacteria, including many pathogens, such as species of *Pseudomonas*, *Vibrio* and *Yersinia* (Vallenet et al., 2013). Moreover, the key residues involved in pppGpp binding (R68, R70, K73, R341, Y347) are highly conserved or conservatively substituted (R68Q, K73R, R341K, Y347F), suggesting that these orthologues are regulated by (p)ppGpp in a similar way as the *E. coli* enzyme (Figures 2F and S2). Finally, structural analysis of the conservation pattern shows that the most conserved regions are located around the catalytic and (p)ppGpp binding sites (Figure S4B). Together, this suggests that regulation of PpnN by the universal stress alarmone (p)ppGpp is a conserved mechanism among Proteobacteria.

(p)ppGpp has a dual effect on purine nucleotide metabolism

The purine nucleotide biosynthesis pathways have been found to be conserved targets of (p)ppGpp in both the Gram-positive Firmicute *B. subtilis* and the Gram-negative Proteobacterium *E. coli* and remarkably, there appear to be both shared and unique targets of (p)ppGpp between these species (Liu et al., 2015a). For example, the *de novo* pathway enzyme GuaB and salvage pathway enzymes Gpt/Hpt are inhibited by (p)ppGpp in both organisms. However, (p)ppGpp inhibits Gmk, the guanylate kinase that converts GMP into GDP, in *B. subtilis*, but not in *E. coli* (Liu et al., 2015b). Here, we found that (p)ppGpp stimulates *E. coli* PpnN, an enzyme highly conserved in Proteobacteria, but absent in Firmicutes. These data thus demonstrate both conserved and differential effects of (p)ppGpp on purine nucleotide biosynthesis enzymes in different phyla of bacteria.

During the stringent response, RNA molecules (including mRNA, rRNA and tRNA) are known to be degraded and stimulatory effect of (p)ppGpp on PpnN probably contributes to the degradation and reuse of these nucleotides (Cashel and Gallant, 1969; Svenningsen et al., 2017). Notably, a recent study has reported a direct inhibitory effect of ppGpp on PurF, the enzyme responsible for the first committed step of the *de novo* purine biosynthesis pathway (Wang et al., 2019). Taken together, the *stimulatory* effect of (p)ppGpp on PpnN activity acts synergistic with the *inhibitory* effect of (p)ppGpp on Gpt/Hpt and GuaB/PurA/PurF, allowing *E. coli* to control the concentration of purine nucleotides during stringent response through both accelerated degradation (PpnN) and reduced biosynthesis (Gpt/Hpt/ GuaB/PurA/PurF). Such a dual effect would result in a dramatic accumulation of nucleobases during stress, which we demonstrated occurs in a *wt*, but not in a Δ*ppnN* strain. Accumulation of nucleobases during stress, such as in stationary phase cells induced by glucose exhaustion or cells experiencing an energy downshift, has been observed previously in *E. coli* (Link et al., 2015; Rinas et al., 1995). Together, this suggests that *E. coli* uses a common mechanism of adjusting nucleotide metabolism when confronted with stress, and that PpnN, being stimulated by

(p)ppGpp, contributes uniquely to this process. Finally, guanine and hypoxanthine, besides serving as resources to support fast regrowth, are also co-repressors of PurR, which downregulates expression of enzymes of the purine *de novo* biosynthesis pathway (Meng and Nygaard, 1990). Thus, the PpnN and (p)ppGpp-dependent accumulation of purine nucleobases may not only deplete the cell of nucleotides, but also repress transcription of genes that are involved in the purine *de novo* pathway.

A model for balancing competitive growth and stress response

We observed that a *wt E. coli* strain out-competes a Δ*ppnN* strain during competitive growth (Figure 4A). On the contrary, a Δ*ppnN* strain complemented by *ppnN*$_{RRK}$ or *ppnN*$_{RY}$ outperforms the *wt* under the same conditions, which is consistent with the observation that the mutant PpnN proteins have a higher basal level of enzymatic activity than *wt* PpnN. Surprisingly, a *wt* strain produces significantly fewer persister cells than Δ*ppnN* during the early phase of growth resumption, while even fewer persisters are observed for both the *ppnN*$_{RRK}$ and *ppnN*$_{RY}$ complemented strains. Taken together, these apparently contradictive behaviours of Δ*ppnN* and those complemented by the mutant *ppnN* alleles lead us to propose a model wherein *E. coli* uses (p)ppGpp to moderate the activities of PpnN and Gpt/Hpt to balance competitive fitness and persistence (Figure 5). Perturbation of such a system by either deletion of *ppnN* or dysregulation of PpnN by removal of the (p)ppGpp regulatory effect results in either high persistence but compromised competitive fitness or highly competitive growth but compromised persistence, respectively. These data suggest that *E. coli*, and probably many other Proteobacteria, have evolved a fine-tuning system comprised of (p)ppGpp and PpnN/Gpt/Hpt that optimises the response to complicated environments of both nutrient and challenges, thus promoting overall ecological survival. Indeed, *ppnN* has been found to be disrupted in an *E. coli* strain isolated from a patient suffering from peritonitis (Launay, 2016) as well as in a *Salmonella* Enteritidis strain isolated from a patient who had been treated with several antibiotics, including ciprofloxacin (Klemm

et al., 2016). In these situations, it is possible that the balance between competitive growth and persistence is shifted in favour of persistence, i.e. that disruption of *ppnN* allows the pathogens to form persister cells with a higher frequency and thus gain fitness during antibiotic treatment. It may even be that stress conditions inside bacterial hosts have selected for the dysfunction of *ppnN,* which again has led to increased bacterial survival and thus, enhanced antibiotic tolerance.

ACKNOWLEDGEMENTS

The authors are thankful to Martin Willemoës for helpful discussions and Sine Nøhr Nielsen for help with refinement of the pppGpp-bound structure. We are also indebted to the beamline staff at Diamond Light Source for help during data collection for the *apo* structure and P13 staff at EMBL in Hamburg for help with data collection for the structure of pppGpp-bound PpnN. This project was funded by an EU Horizon 2020 Marie Sklodowska-Curie grant (no. 707138) to Y.Z., an ERC Advanced Investigator grant (PERSIST 294517 to K.G.), and grants from the Novo Nordisk Foundation (to both K.G. and D.E.B.) and the Danish Natural Research Foundation (DNRF 120).

AUTHOR CONTRIBUTIONS

Conceptualization, Y.Z., K.G., and D.E.B.; Investigation, Y.Z., R.L.B., and T.F.; Formal Analysis, Y.Z. and R.L.B; Writing – Original Draft, Y.Z., K.G., R.L.B., and D.E.B.; Writing – Review & Editing, Y.Z., R.L.B., T.F., U.S., K.G., and D.E.B; Visualization, Y.Z., R.L.B., and D.E.B.; Funding Acquisition, Y.Z., K.G., and D.E.B.; Resources, Y.Z., U.S., K.G., and D.E.B; Supervision, Y.Z. and D.E.B.

DECLARATIONS OF INTERESTS

The authors declare no competing interests.

FIGURE TITLES AND LEGENDS

Figure 1. (p)ppGpp stimulates the catalytic activity of PpnN. A. Overview of the purine nucleotide biosynthesis and degradation pathways, including the regulatory effects of (p)ppGpp on some enzymes in *E. coli*. Black arrows indicate biochemical reactions; green and red lines indicate positive and negative regulatory effects of (p)ppGpp on specific enzymatic activities, respectively, with dotted and solid lines indicating weak and strong effects, respectively. PRPP, 5'-phosphoribosyl 1'-pyrophosphate; Gln, glutamine. **B.** Details of the biochemical reaction catalysed by *E. coli* PpnN. The green arrow indicates positive regulation by (p)ppGpp. **C.** Kinetic analysis of *E. coli* PpnN as measured by untargeted mass spectrometry with GMP as substrate in the absence or presence of 100 μM pppGpp or ppGpp as indicated. The data are represented by mean ± SEM. **D.** Normalised (per OD_{600}) guanine (m/z = 150.0421) (solid lines) and xanthine (m/z = 151.0266) (dashed lines) abundances before (time 0 min) and after valine-induced isoleucine starvation in MOPS media as measured for both *E. coli wt* (black) and *ΔppnN* (red) by untargeted mass spectrometry. Three biological replicates were performed for the wild type (*wt*) and *ΔppnN* strains, and the data are represented by mean ± SEM. *, Student's *t* test $p<0.05$. See also Figure S1.

Figure 2. *E. coli* PpnN forms a tetramer with an allosteric (p)ppGpp binding site. A. Overview of the PpnN monomer structure, with the N-terminal DUF4478 (red), catalytic (purple), and C-terminal DUF3412 (blue) domains shown in individual colours. Putative active site residues are shown in yellow sticks and indicated with a dashed, semi-transparent circle. A schematic overview of the protein sequence is shown below. **B.** Overview of the PpnN tetramer (*apo* form) with the dimer present in the crystallographic asymmetric unit (a.s.u.) shown in the dashed square. The two internal 2-fold axes of the tetramer are indicated by lines with longer dashes while the circled grey areas

indicate the location of the interacting 67-72/343-348 loops as well as (p)ppGpp binding sites between monomers (two sites per circle). **C.** Details of the pppGpp-binding site found between the N-terminal (DUF4478) and C-terminal (DUF3412) domains in the *apo* structure with relevant residues highlighted. **D.** Details of the pppGpp binding site with relevant residues highlighted and the 342-345 region indicated. pppGpp is shown in green/orange coloured sticks with key interactions to the protein indicated by dashed lines. **E.** Details of the interactions between PpnN and pppGpp. Cyan circles indicate water molecules. The figure was produced using Ligplot (Wallace et al., 1995). **F.** Sequence alignment of residues involved in pppGpp binding in PpnN homologs from 12 representative Proteobacteria. Pa, *Pseudomonas aeruginosa* PA01; Vc, *Vibrio cholerae* N16961; Ah, *Aeromonas hydrophila* ATCC 7966; Kp, *Klebsiella pneumoniae* 1084; So, *Shewanella oneidensis* MR-1; Ck, *Citrobacter koseri* ATCC BAA-895; Av, *Aeromonas veronii* B565; Ed, *Enterobacter dissolvens* SDM; St, *Salmonella typhimurium* SL1344; Ec, *Escherichia coli* K12; Sf, *Shigella flexneri* 2a 301, Yp, *Yersinia pestis* KIM. Asterisks (*) indicate residues directly coordinating pppGpp in *E. coli* PpnN. See also Figures S2 and S3.

Figure 3. pppGpp binding involves conserved basic residues and induces a conformational change. A. Comparison of the pppGpp-bound structure of PpnN (shown with colours) with the *apo* structure (grey) showing that pppGpp binding induces a large conformational change (indicated with arrows), increasing access to the active site (dashed, semi-transparent circle). Each monomer is involved in binding two molecules of pppGpp at its interfaces with adjacent molecules (bottom and right). The 50 and 400 loops that interact in the *apo* form are indicated. **B**. Overview of the dimer interface focusing on a single pppGpp binding site. pppGpp is shown with sticks coloured by atom while the residues required for binding in each subunit (RRK, green; RY, magenta) are shown in single colours. **C.** DRaCALA binding curves of α-^{32}P-pppGpp to *wt* and mutant PpnN proteins. The

485 curves were fit using a non-linear one-site total binding model in GraphPad Prism. At least three
486 replicates were performed for each reaction and data are represented by mean ± SEM. **D.** Fold
487 stimulation of enzymatic activity upon addition of 100 μM pppGpp and initial reaction velocities
488 (relative to *wt*) of *wt* and mutant PpnN proteins measured by XMP degradation (see main text). Three
489 replicates were performed and the data are represented by mean ± SEM. See also Figure S4.
490
491 **Figure 4. (p)ppGpp and PpnN affect *E. coli* fitness and persister levels. A.** Fractional change of
492 Δ*ppnN* cells during competitive growth with *wt lacZ:kan* in LB-B broth (see STAR Methods for
493 details). Log, maintenance of the mixed cells in log phase in LB-B broth (see main text for details);
494 Log – Stat, periodical (every 24 h) sub-culturing of mixed stationary phase cells starting from
495 OD_{600}=0.005 in fresh LB-B broth. **B.** Regrowth curves showing the number of colony-forming units
496 (CFUs, x10_7/ml, in grey) and the percentage of persisters after ofloxacin (5 μg/ml) exposure for the
497 *wt*, Δ*ppnN*, and an *in situ* complemented strain Δ*ppnN::ppnN*$_{wt}$ during growth resumption in LB-B
498 broth from 16 h overnight cultures. Phase I denotes the period from the beginning of regrowth period
499 to mid-log phase (0-2 h) and phase II the transition to stationary phase (2-5 h). **C.** Fractional change
500 of Δ*ppnN*, Δ*ppnN::ppnN*$_{wt}$, Δ*ppnN::ppnN*$_{RRK}$ and Δ*ppnN::ppnN*$_{RY}$ during competitive growth with
501 wt *lacZ:kan* in LB-B broth under the Log – Stat scheme as in **A**. **D.** As **B** but using strains
502 complemented with the Δ*ppnN::ppnN*$_{RRK}$ and Δ*ppnN::ppnN*$_{RY}$ mutants during growth resumption in
503 LB-B broth from 16 h overnight cultures. For all experiments, at least three biological replicates were
504 performed and the data are represented by mean ± SEM. * and ** indicate Student's *t* test $p<0.05$ and
505 $p<0.01$, respectively. See also Figure S5.
506
507 **Figure 5. Model for balancing competitive growth and antibiotic tolerance via the dual effects**
508 **of (p)ppGpp.** *E. coli* uses (p)ppGpp to simultaneously stimulate PpnN and inhibit Gpt/Hpt to regulate

509 purine nucleotide metabolism and balance competitive growth and antibiotic tolerance. The upper
510 (dashed black) line indicates one extreme scenario (demonstrated by Δ*ppnN*) where the balance is
511 shifted in favour of enhanced antibiotic tolerance, while the lower (solid black) line shows the other
512 extreme (demonstrated by the *ppnN*$_{RRK}$ and *ppnN*$_{RY}$ mutants) where competitive growth is prioritised.
513 G, guanine; X, xanthine; H, hypoxanthine; R5P, ribose-5'-phosphate.
514

Table 1. Crystallographic data statistics.

	apo	pppGpp-bound
Data Collection		
Wavelength (Å)	0.9686	0.97623
Resolution range (Å)	49.1 – 2.48 (2.57 – 2.48)*	34.7 – 2.77 (2.87 – 2.77)
Space group	$P2_12_12$	$I4_122$
Unit cell dimensions		
a, b, c, (Å)	94.2, 101.1, 112.3	176.9, 176.9, 94.5
α, β, γ (o)	90, 90, 90	90, 90, 90
Total reflections	77,132 (7597)	479,668 (34,795)
Unique reflections	38,643 (3810)	19,332 (1907)
Multiplicity	13.4 (7.4)	24.8 (18.2)
Completeness (%)	99.9 (99.9)	99.8 (99.7)
R_{merge} (%)	4.0 (61)	14.2 (270)
I/σ(I)	10.3 (1.2)	17.5 (1.4)
$CC_{1/2}$	1.00 (0.59)	1.00 (0.58)
Refinement		
Average B-factor ($Å_2$)	92.8	102.7
No. of reflections	38,638 (3810)	19,329 (1906)
No. of reflections (free)	1878 (171)	895 (87)
R (%)	21.2 (33.0)	18.1 (34.3)
R_{free} (%)	26.9 (38.0)	23.2 (37.1)
Number of		
protein (residues)	860	440
solvent (atoms)	161	99
ligand (atoms)	-	40
rmsd bonds lengths (Å)	0.004	0.002
rmsd bond angles (o)	0.72	0.48
Ramachandran statistics		
Favoured (%)	96.6	95.0
Allowed (%)	3.0	5.0
Outliers (%)	0.4	0.0

*Numbers in parentheses refer to the outermost resolution shell.

STAR METHODS

CONTACT FOR REAGENT AND RESOURCE SHARING

Further information and requests for resources and reagents should be directed to and will be fulfilled by Ditlev E. Brodersen (deb@mbg.au.dk).

EXPERIMENTAL MODEL AND SUBJECT DETAILS

E. coli DH5α (Stratagene) was used for cloning, *E. coli* BL21 (DE3) (Novagen) for protein expression, and MG1655 for experiments requiring an *E. coli* wild type strain background (see Table S1 for further details). For cloning and protein expression for biochemistry, nutrient broth (Oxoid), with agar when appropriate, was used while LB Broth (Sigma Aldrich) supplemented with 34 μg/μL chloramphenicol was used for structural studies. For metabolomics analysis and autoradiography, MOPS media (Neidhardt et al., 1974) supplemented with 0.2% (g/ml) glucose and a low concentration (0.2 mM) of Na_2HPO_4 was used. The experiments of growth resumption, competitive fitness and persistence were performed in LB-B broth, containing 10 g tryptone (Oxoid), 5 g yeast extract (Oxoid), and 10 g NaCl per liter with pH adjusted to 7.43. When appropriate, chloramphenicol (25 μg/ml), ampicillin (100 μg/ml), and/or kanamycin (25 μg/ml) were used.

METHOD DETAILS

Plasmids constructions

To construct the plasmids pCA24N-PpnN(R68A), pCA24N-PpnN(R70A), pCA24N-PpnN(K73A), pCA24N-PpnN(R68R70K73AAA), pCA24N-PpnN(R341A), pCA24N-PpnN(Y347A) and pCA24N-PpnN(R341AY347A), quick-change mutagenesis was carried out using pCA24N-PpnN(wt) as template (Kitagawa et al., 2005) and the primer pairs PYZ248/249, PYZ250/251, PYZ252/253, PYZ254/255, PYZ256/257, PYZ258/259 and PYZ260/261, respectively (see Table S2

for details of primers). All plasmids were purified from *E. coli* DH5α and confirmed by sequencing (primers PYZ34/35, Eurofins genomics). For protein expression and purification, individual plasmids were transformed into *E. coli* BL21(DE3) (see Table S1 for details). The in-frame scar-less deletion mutant *ΔppnN*(YZ364) was constructed by using I-*Sce*I-based λ-Red recombineering essentially as reported before (Blank et al., 2011). Briefly, primers PYZ273/274 were used to amplify the SceI-Cam fragment from the pWRG100 plasmid, which was electroporated into MG1655 containing pWRG99 (YZ309). Annealed primers PYZ283/284 were then used to delete the *ppnN* sequence from codon 29 to the stop codon. For complementation of *ΔppnN*, primers PYZ273/285 were used to amplify the SceI-Cam fragment from the pWRG100 plasmid, which was electroporated into the *ΔppnN* strain containing pWRG99 (YZ362). Subsequently, primer pairs PYZ212/213 (for wt *ppnN* allele), PYZ254/PYZ213 and PYZ255/PYZ212 (for *ppnN(RRK)* allele), PYZ260/PYZ213 and PYZ261/PYZ212 (for *ppnN(RY)* allele) were used to amplify either *wt* or mutant *ppnN* alleles to be electroporated into YZ362 to obtain *in situ* complemented strains. The respective *ppnN* sequences of the complemented strains were confirmed by PCR amplification and sequencing.

Synthesis of α-^{32}P-(p)ppGpp and DRaCALA binding assays

α-^{32}P-labelled pppGpp was synthesized from α-^{32}P-GTP (PerkinElmer) by incubating 125 nM α-^{32}P-GTP with 4 μM purified RelSeq-His protein in a reaction buffer containing 25 mM Tris pH 9.0, 100 mM NaCl, 15 mM $MgCl_2$, and 8 mM ATP at 37°C for 1 h (Mechold et al., 2002). The sample was heated for 5 min at 95°C to stop the synthesis, and the denatured RelSeq-His protein removed by centrifugation at 14,000 rpm for 10 min at 4°C. The supernatant containing α-^{32}P-pppGpp was transferred to a new tube. For synthesis of α-^{32}P-ppGpp, half of the synthesized α-^{32}P-pppGpp was added with 1 μM purified GppA-His protein. The reaction was performed at 37°C for 15 min before been heat inactivated for 5 min at 95°C, and the denatured GppA-His protein removed by

centrifugation. The ratios of the conversion of α-^{32}P-GTP to α-^{32}P-pppGpp and of α-^{32}P-pppGpp to α-^{32}P-ppGpp were determined to be more than 92%, as assessed by thin-layer chromatography (TLC) using 1.5 M KH_2PO_4 (pH 3.4) as the mobile phase (Zhang et al., 2018). For K_d measurements by the DRaCALA binding assay, two-fold serial dilutions of the purified wild type and mutant PpnN proteins (starting from 40 μM) were prepared in the binding buffer (containing 40 mM Tris pH 7.5, 100 mM NaCl, 100 mM KCl), and α-^{32}P-labeled ppGpp or pppGpp were added to a final concentration of ~2 nM. The mixtures were incubated for 5 min at RT and 2 μl was spotted on nitrocellulose membranes. The fractions of bound ligand and the apparent K_d values were calculated as previously described (Roelofs et al., 2011).

Biochemical assays of PpnN activity and the effects of (p)ppGpp

The use of XMP as substrate for PpnN and assayed with spectrometry is based on (Arent et al., 2006). The conversion between XMP and xanthine cause large spectral changes due to the differential pK_a values of the two molecules, but an isosbestic point at 252 nm was found where the difference in the absorbance of XMP and xanthine does not change under different pH values. Although both ppGpp and pppGpp show absorption at 252 nm, the changes in absorbance due to spontaneous self-decay of (p)ppGpp were trivial and could be deducted before fitting. For conversion of XMP to xanthine, 10 nM wt or mutant His_6-PpnN and 25 μM XMP were used in a reaction buffer containing 50 mM Tris-HCl pH 7.5, 100 mM NaCl, 1 mM $MgCl_2$. The reactions were performed at 37°C in microtitre plates (Greiner UV-Star) and spectral changes at 252 nm monitored by using Biotek Synergy H1 plate reader over ten minutes. To test the effects of ppGpp and pppGpp (BioLog) on PpnN activity, 100 μM of each was used. The kinetics of PpnN activity was measured using GMP as substrate. For this, 50 nM of freshly purified His_6-PpnN was incubated with 2-fold serial diluted GMP (from 2 mM to 62.5 uM) in the reaction buffer containing 50 mM Tris-HCl pH 8.0 and 1 mM $MgCl_2$. To test the

590 effects of (p)ppGpp on the PpnN kinetics, 100 µM of each was used. Heat-inactivated His_6-PpnN was
591 used as negative control, which confirmed the absence of degradation of either GMP or (p)ppGpp
592 during the reaction (5 min). Reactions were performed at 37°C in a heat block and stopped after 1, 2,
593 or 5 min by mixing one portion of the reaction solution with four portions of 100% methanol pre-
594 cooled on dry ice. The reactions were characterised and the products quantified by untargeted mass
595 spectrometry as described previously (Fuhrer et al., 2011).
596
597 **Metabolomics analysis of nucleotides**
598 The fast filtration method was used to harvest cells and extract metabolites as described previously
599 (Link et al., 2013). Briefly, *wt* and *ΔppnN E. coli* strains were grown in MOPS medium supplemented
600 with 0.2% (g/ml) glucose and 0.2 mM of Na_2HPO_4 (referred to as "MOPS medium" here) to
601 saturation overnight. Each culture was then sub-cultured in fresh MOPS medium starting from
602 OD_{600}=0.025. When the OD_{600} reached approx. 0.16 (~4 h), valine stock (5 mg/ml) was added to the
603 cultures to a final concentration of 500 µg/ml. Right before and 5, 10, 20, 40 min after addition of
604 valine, 8 ml of each culture was harvested and immediately washed with 16 ml of ice cold 10 mM
605 ammoniumcarbonate pH 7.2. Simultaneously, the OD_{600} was measured. The filters with collected
606 cells were immersed in 4 ml of the extraction solution containing 40%:40%:20% (by volume) of
607 acetonitrile:methanol:MiliQ water, in a Falcon tube precooled on dry ice, and the metabolites were
608 extracted overnight at -20^{o}C. The next day, the extracted metabolites were collected by centrifuging
609 at 4000 rpm for 10 min at 4^{o}C. Another 4 ml of extraction buffer was used to wash the extraction tube
610 and combined with the first extraction. The metabolites were then freeze-dried before being analysed
611 with untargeted MS as described (Fuhrer et al., 2011).
612
613 **Measurements of (p)ppGpp by autoradiography**

(p)ppGpp is a highly labile molecule not amenable to HPLC or mass spectrometry analysis (Varik et al., 2017). Therefore, thin layer chromatography (TLC) was used to quantify both pppGpp and ppGpp. For this, both *wt* and *ΔppnN E. coli* strains were grown to early log phase (OD_{600} ~0.1) in MOPS medium. Then, $H_3{}^{32}PO_4$ (100 µCi/ml, PerkinElmer) was added and the cultures incubated at 37°C (600 rpm) for 40 min in a thermomixer (Eppendorf). Valine was added to a final concentration of 500 µg/ml to induce isoleucine starvation. Identical cultures, except without the addition of $H_3{}^{32}PO_4$, were kept in parallel to measure the OD_{600}. Right before and 2, 4, 8, and 16 min after starvation, 50 µl of cultures were removed to mix with 10 µl ice cold 2 N formic acid and left for 15 min on ice or stored at -20°C before resolving on TLC using 1.5 M KH_2PO_4 (pH 3.4) as the mobile phase (Zhang et al., 2018).

Competitive growth assay

For the Log-Stat scheme, the OD_{600} of overnight cultures of each strain was measured and an equal number of each cells were mixed together in appropriate combinations. The mixed cells were washed once with 1x Phosphate Buffered Saline (PBS) and inoculated into fresh LB-B broth with starting OD_{600}=0.005. The initial fractions of each combined strain were determined by serial dilution of the mixed cells and plated on X-gal containing LB agar plates. After every 24 h of co-growth at 37°C with agitation (160 rpm), the mixed cells were re-inoculated by 1/1000 dilution in fresh LB-B broth and the fractions of each strain in the populations were similarly determined. For the Log scheme, overnight cultures of each strain were first sub-cultured in fresh LB-B broth to early log phase after which the OD_{600} was measured and an equal number of cells were mixed in appropriate combinations. The mixed cells were directly inoculated into fresh LB-B broth starting from OD_{600}=0.005. After every 2 h of co-growth at 37°C with agitation (160 rpm) (approx. 6 generations), the mixed cells were

637 re-inoculated into fresh LB-B broth starting from OD_{600}=0.005. The fraction of each strain in the
638 populations were determined similarly as above.
639
640 **Persistence assay**
641 The experimental setup is similar to (Harms et al., 2017). Briefly, a 16 h overnight culture of each
642 strain was made in 2 ml LB-B broth in a snap-tube (Sarstedt, no. 62.515.006) from which 120 µl of
643 cells were inoculated into each of a series of 125 ml flasks containing 12 ml fresh LB-B broth at room
644 temperature. Cells were grown in a water bath at 37°C with agitation (160 rpm). After each hour (up
645 to 5/8 h), 2 ml of cells were removed to a snap-tube containing lethal concentrations of antibiotics
646 (100 µg/ml ampicillin, 7.5 µg/ml gentamicin, 5 µg/ml ofloxacin, or 10 µg/ml ciprofloxacin) and
647 incubated at 37°C with agitation (160 rpm). Meanwhile, the total number of colony-forming units
648 (CFUs) before exposure to antibiotics was determined by serial dilution, spotting and incubation at
649 37°C for 24 h before counting. After 5 h of antibiotic killing, 1.4 ml of cells was removed to an
650 Eppendorf tube and spun down at 5000 rpm 3 min and then 14000 rpm 2 min. Cells were washed
651 once with 1 ml of PBS and spun down as above. The supernatant was removed completely after a
652 final spin at 14000 rpm for 2 min and the pelleted cells were resuspended in PBS, serial diluted and
653 spotted on LB agar plate to measure the number of persisters, again by determining the CFUs. For
654 time zero samples, 2 ml of the inoculated cells were immediately removed and exposed to antibiotics
655 and the total CFUs before and after antibiotic killing were determined as above.
656
657 **Western blots**
658 Western blot analysis of PpnN expression was performed as reported (Zhang et al., 2017). Briefly, *E.*
659 *coli* cells collected either during valine-induced isoleucine starvation in MOPS media or during
660 regrowth in LB-B broth were normalised to an equal OD_{600} per ml and mixed with 2x SDS-PAGE

loading buffer. Samples were heated for 15 min at 95°C and 20 µl of each were separated in 4-12% Bis-Tris NuPAGE gels (Invitrogen). The proteins were transferred to a PVDF membrane (Amersham) and proteins detected by first incubation with anti-PpnN antiserum (Covalab) and HRP conjugated rabbit IgG antibody (Sigma) as secondary antibody. Bands were visualised by using the Pierce ECL chemiluminescence substrate (Thermo) and signals were quantified using an Imagequant LAS4100.

Protein Purification, crystallisation, and structure determination

Expression of the N-terminal hexa-histidine tagged PpnN was induced with 1 mM IPTG at a cell density of OD_{600}=0.3. 2 L of cells were pelleted, suspended in lysis buffer (50 mM Tris-HCl pH 7.5, 300 mM NaCl, 10 mM imidazole, 5% glycerol, 5 mM BME), lysed by sonication, and purified in three steps using a HisTrap HP column (GE Healthcare) washed in 50 mM Tris-HCl pH 7.5, 300 mM NaCl, 20 mM imidazole, 5 mM BME before eluting with 50 mM Tris-HCl pH 7.5, 300 mM NaCl, 200 mM imidazole, 5 mM BME. The eluted sample was diluted in 50 mM Tris-HCl pH 9, 5 mM BME to ~100 mM NaCl, loaded onto a 1 ml Source 15Q (GE Healthcare) ion exchange column, and eluted with a gradient into 50 mM Tris-HCl pH 9, 1 M NaCl, 5 mM BME. Final separation was achieved using a Superdex 200 10/300 GL (GE Healthcare) column equilibrated in 20 mM Tris-HCl pH 7.5, 100 mM NaCl, 5 mM BME. Crystals of *apo* PpnN grew in sitting drops containing 1 µL of 4.25 mg/ml purified protein and 2 µL of 0.1M Hepes pH 7.5, 36% v/v PEG 200 at 293 K. For the pppGpp-bound form, the purified protein at 7 mg/ml was pre-incubated with 1 mM pppGpp (Jena Bioscience) and incubated for 1 hour at 4°C before mixing 1:1 (v/v) with 0.4 M KNa tartrate tetrahydrate and set to equilibrate at 273K in sitting drops. All crystals were cryoprotected by the addition of 30% v/v glycerol and frozen directly in liquid N_2. The data of *apo* PpnN were collected at Diamond Light Source, while the data for the pppGpp-bound PpnN were collected at P13 at EMBL in Hamburg. Data were indexed, integrated, and scaled using XDS/XSCALE (Kabsch, 2010).

Molecular replacement was carried out using Phaser, and model-building (protein+ligand) and refinement was done iteratively using Phenix.refine and Coot (Adams et al., 2010; Emsley and Cowtan, 2004). Phases for the *apo* form of PpnN were obtained by molecular replacement using a homolog from *V. cholerae* (PDB ID: 2PMB) as search model, while phases for the pppGpp-bound PpnN were obtained using the *apo* structure as search model. Both structures were validated using the output from the MolProbity server and structural conservation was analysed using Consurf (Landau et al., 2005).

Bioinformatics analysis

The protein sequence of *E. coli* PpnN protein was used to retrieve sequences of a total of 668 PpnN orthologues (with minimum 30% amino acid identity and 90% coverage) from the Genoscope database (http://www.genoscope.cns.fr). Multiple sequence alignment using ClustalO in Jalview was performed with 12 representative sequences of PpnN from *Pseudomonas aeruginosa* PA01, *Vibrio cholerae* N16961, *Aeromonas hydrophila* ATCC 7966, *Klebsiella pneumoniae* 1084, *Shewanella oneidensis* MR-1, *Citrobacter koseri* ATCC BAA-895, *Aeromonas veronii* B565, *Enterobacter dissolvens* SDM, *Salmonella typhimurium* SL1344, *Escherichia coli* K12, *Shigella flexneri* 2a 301, and *Yersinia pestis* KIM.

QUANTIFICATION AND STATISTICAL ANALYSIS

For biochemical analyses of the effects of (p)ppGpp on PpnN activity using XMP as substrate, at least three replicates were performed for each reaction and spectrometry (change of absorption at 252 nm) was used to monitor the reactions. Linear regression was applied to obtain initial velocities with GraphPad Prism. For kinetics analysis of PpnN using GMP as substrate, untargeted mass spectrometry was used to characterize the reactions (Fuhrer et al., 2011). Two replicates were done

for each reaction and the data fitted with a non-linear allosteric sigmoidal model using GraphPad Prism. Student's *t*-test was used for statistics of both experiments.

For metabolomics analysis, the abundance of extracted metabolites were determined by mass spectrometry as in (Link et al., 2013). The final relative abundance of each metabolite was normalised to measured OD_{600} values and expressed as ion counts per OD_{600}. Three biological replicates were performed for each strain and Student's *t*-test was used to check for statistical significance.

Signals of pppGpp and ppGpp from autoradiography were quantified using ImageQuant (GE Healthcare) and normalised to measured OD_{600} values. At least three biological replicates were performed and one representative shown.

For the competitive growth assay, two different combinations of experiments, either using *wt* or *wt lacZ:kan E. coli* strains, were performed in at least three biological replicates. For the persistence assay, the percentage of persisters was calculated by dividing the number of CFUs after exposure to antibiotics by the value before exposure. At least three biological replicates were performed for each strain and Student's *t*-test was used for statistics.

DATA AND SOFTWARE AVAILABILITY

The structures of PpnN deposited in the Protein Data Bank under ID codes 6GFL (*apo* form) and 6GFM (pppGpp-bound form).

SUPPLEMENTAL MATERIAL

Movie S1. Visualisation of the domain organisation of *E. coli* PpnN and structural changes upon pppGpp binding, Related to Figures 2 and 3. The movie shows an overview of the tetrameric state of E. coli PpnN, then highlights the three domains of each monomer using different colours. pppGpp binding is shown along with the structural changes it induces in the protein both at the global and local levels. Finally, a close-up view of the pppGpp binding site shows the RRK and RY residues involved in binding the ligand.

REFERENCES

Adams, P.D., Afonine, P.V., Bunkoczi, G., Chen, V.B., Davis, I.W., Echols, N., Headd, J.J., Hung, L.W., Kapral, G.J., Grosse-Kunstleve, R.W.*, et al.* (2010). PHENIX: a comprehensive Python-based system for macromolecular structure solution. Acta Crystallogr D Biol Crystallogr *66*, 213-221.

Arent, S., Kadziola, A., Larsen, S., Neuhard, J., and Jensen, K.F. (2006). The extraordinary specificity of xanthine phosphoribosyltransferase from Bacillus subtilis elucidated by reaction kinetics, ligand binding, and crystallography. Biochemistry *45*, 6615-6627.

Balaban, N.Q., Merrin, J., Chait, R., Kowalik, L., and Leibler, S. (2004). Bacterial persistence as a phenotypic switch. Science *305*, 1622-1625.

Baugh, L., Phan, I., Begley, D.W., Clifton, M.C., Armour, B., Dranow, D.M., Taylor, B.M., Muruthi, M.M., Abendroth, J., Fairman, J.W.*, et al.* (2015). Increasing the structural coverage of tuberculosis drug targets. Tuberculosis (Edinb) *95*, 142-148.

Bennett, B.D., Kimball, E.H., Gao, M., Osterhout, R., Van Dien, S.J., and Rabinowitz, J.D. (2009). Absolute metabolite concentrations and implied enzyme active site occupancy in Escherichia coli. Nat. Chem. Biol. *5*, 593-599.

Blank, K., Hensel, M., and Gerlach, R.G. (2011). Rapid and highly efficient method for scarless mutagenesis within the Salmonella enterica chromosome. PLoS One *6*, e15763.

Bonanno, J.B., Almo, S.C., Bresnick, A., Chance, M.R., Fiser, A., Swaminathan, S., Jiang, J., Studier, F.W., Shapiro, L., Lima, C.D.*, et al.* (2005). New York-Structural GenomiX Research Consortium

(NYSGXRC): a large scale center for the protein structure initiative. J Struct Funct Genomics *6*, 225-232.

Cashel, M., and Gallant, J. (1969). Two compounds implicated in the function of the RC gene of Escherichia coli. Nature *221*, 838-841.

Dalebroux, Z.D., Svensson, S.L., Gaynor, E.C., and Swanson, M.S. (2010). ppGpp conjures bacterial virulence. Microbiol. Mol. Biol. Rev. *74*, 171-199.

Dzurova, L., Forneris, F., Savino, S., Galuszka, P., Vrabka, J., and Frebort, I. (2015). The three-dimensional structure of "Lonely Guy" from Claviceps purpurea provides insights into the phosphoribohydrolase function of Rossmann fold-containing lysine decarboxylase-like proteins. Proteins *83*, 1539-1546.

Emsley, P., and Cowtan, K. (2004). Coot: model-building tools for molecular graphics. Acta Crystallogr D Biol Crystallogr *60*, 2126-2132.

Fridman, O., Goldberg, A., Ronin, I., Shoresh, N., and Balaban, N.Q. (2014). Optimization of lag time underlies antibiotic tolerance in evolved bacterial populations. Nature *513*, 418-421.

Fuhrer, T., Heer, D., Begemann, B., and Zamboni, N. (2011). High-throughput, accurate mass metabolome profiling of cellular extracts by flow injection-time-of-flight mass spectrometry. Anal Chem *83*, 7074-7080.

Gerhart, J.C., and Schachman, H.K. (1965). Distinct subunits for the regulation and catalytic activity of aspartate transcarbamylase. Biochemistry *4*, 1054-1062.

Harms, A., Fino, C., Sørensen, M.A., Semsey, S., and Gerdes, K. (2017). Prophages and Growth Dynamics Confound Experimental Results with Antibiotic-Tolerant Persister Cells. MBio *8*.

Harms, A., Maisonneuve, E., and Gerdes, K. (2016). Mechanisms of bacterial persistence during stress and antibiotic exposure. Science *354*.

Hauryliuk, V., Atkinson, G.C., Murakami, K.S., Tenson, T., and Gerdes, K. (2015). Recent functional insights into the role of (p)ppGpp in bacterial physiology. Nat. Rev. Microbiol. *13*, 298-309.

783 Hochstadt-Ozer, J., and Cashel, M. (1972). The regulation of purine utilization in bacteria. V.
784 Inhibition of purine phosphoribosyltransferase activities and purine uptake in isolated membrane
785 vesicles by guanosine tetraphosphate. J. Biol. Chem. *247*, 7067-7072.

786 Kabsch, W. (2010). Xds. Acta Crystallogr D Biol Crystallogr *66*, 125-132.

787 Kanjee, U., Gutsche, I., Alexopoulos, E., Zhao, B., El Bakkouri, M., Thibault, G., Liu, K.,
788 Ramachandran, S., Snider, J., Pai, E.F.*, et al.* (2011). Linkage between the bacterial acid stress and
789 stringent responses: the structure of the inducible lysine decarboxylase. EMBO J. *30*, 931-944.

790 Kitagawa, M., Ara, T., Arifuzzaman, M., Ioka-Nakamichi, T., Inamoto, E., Toyonaga, H., and Mori,
791 H. (2005). Complete set of ORF clones of Escherichia coli ASKA library (A complete Set of E. coli
792 K-12 ORF archive): Unique resources for biological research. DNA Res. *12*, 291-299.

793 Klemm, E.J., Gkrania-Klotsas, E., Hadfield, J., Forbester, J.L., Harris, S.R., Hale, C., Heath, J.N.,
794 Wileman, T., Clare, S., Kane, L.*, et al.* (2016). Emergence of host-adapted Salmonella Enteritidis
795 through rapid evolution in an immunocompromised host. Nat. Microbiol. *1*, 15023.

796 Krissinel, E., and Henrick, K. (2007). Inference of macromolecular assemblies from crystalline state.
797 J. Mol. Biol. *372*, 774-797.

798 Landau, M., Mayrose, I., Rosenberg, Y., Glaser, F., Martz, E., Pupko, T., and Ben-Tal, N. (2005).
799 ConSurf 2005: the projection of evolutionary conservation scores of residues on protein structures.
800 Nucleic Acids Res. *33*, W299-302.

801 Launay, A. (2016). Study of the emergence of the diversity of Escherichia coli in vivo by whole
802 genome sequencing. (Université Pierre et Marie Curie - Paris VI).

803 Leavitt, R.I., and Umbarger, H.E. (1962). Isoleucine and valine metabolism in Escherichia coli. XI.
804 Valine inhibition of the growth of Escherichia coli strain K-12. J. Bacteriol. *83*, 624-630.

805 Link, H., Fuhrer, T., Gerosa, L., Zamboni, N., and Sauer, U. (2015). Real-time metabolome profiling
806 of the metabolic switch between starvation and growth. Nat. Methods *12*, 1091-1097.

807 Link, H., Kochanowski, K., and Sauer, U. (2013). Systematic identification of allosteric protein-
808 metabolite interactions that control enzyme activity in vivo. Nat. Biotechnol. *31*, 357-361.

809 Liu, K., Bittner, A.N., and Wang, J.D. (2015a). Diversity in (p)ppGpp metabolism and effectors. Curr.
810 Opin. Microbiol. *24*, 72-79.

811 Liu, K., Myers, A.R., Pisithkul, T., Claas, K.R., Satyshur, K.A., Amador-Noguez, D., Keck, J.L., and
812 Wang, J.D. (2015b). Molecular mechanism and evolution of guanylate kinase regulation by
813 (p)ppGpp. Mol. Cell *57*, 735-749.

814 Lopez, J.M., Dromerick, A., and Freese, E. (1981). Response of guanosine 5'-triphosphate
815 concentration to nutritional changes and its significance for Bacillus subtilis sporulation. J. Bacteriol.
816 *146*, 605-613.

817 Mechold, U., Murphy, H., Brown, L., and Cashel, M. (2002). Intramolecular regulation of the
818 opposing (p)ppGpp catalytic activities of Rel(Seq), the Rel/Spo enzyme from Streptococcus
819 equisimilis. J. Bacteriol. *184*, 2878-2888.

820 Meng, L.M., and Nygaard, P. (1990). Identification of hypoxanthine and guanine as the co-repressors
821 for the purine regulon genes of Escherichia coli. Mol. Microbiol. *4*, 2187-2192.

822 Neidhardt, F.C., Bloch, P.L., and Smith, D.F. (1974). Culture medium for enterobacteria. J. Bacteriol.
823 *119*, 736-747.

824 Orr, M.W., and Lee, V.T. (2017). Differential Radial Capillary Action of Ligand Assay (DRaCALA)
825 for High-Throughput Detection of Protein-Metabolite Interactions in Bacteria. Methods Mol Biol
826 *1535*, 25-41.

827 Pao, C.C., and Dyess, B.T. (1981). Effect of unusual guanosine nucleotides on the activities of some
828 Escherichia coli cellular enzymes. Biochim. Biophys. Acta *677*, 358-362.

829 Rinas, U., Hellmuth, K., Kang, R., Seeger, A., and Schlieker, H. (1995). Entry of Escherichia coli
830 into stationary phase is indicated by endogenous and exogenous accumulation of nucleobases. Appl.
831 Environ. Microbiol. *61*, 4147-4151.

832 Roelofs, K.G., Wang, J., Sintim, H.O., and Lee, V.T. (2011). Differential radial capillary action of
833 ligand assay for high-throughput detection of protein-metabolite interactions. Proc. Natl. Acad. Sci.
834 U S A *108*, 15528-15533.

Ross, W., Sanchez-Vazquez, P., Chen, A.Y., Lee, J.H., Burgos, H.L., and Gourse, R.L. (2016). ppGpp Binding to a Site at the RNAP-DksA Interface Accounts for Its Dramatic Effects on Transcription Initiation during the Stringent Response. Mol. Cell *62*, 811-823.

Sevin, D.C., Fuhrer, T., Zamboni, N., and Sauer, U. (2017). Nontargeted in vitro metabolomics for high-throughput identification of novel enzymes in Escherichia coli. Nat. Methods *14*, 187-194.

Steinchen, W., and Bange, G. (2016). The magic dance of the alarmones (p)ppGpp. Mol. Microbiol. *101*, 531-544.

Svenningsen, S.L., Kongstad, M., Stenum, T.S., Munoz-Gomez, A.J., and Sorensen, M.A. (2017). Transfer RNA is highly unstable during early amino acid starvation in Escherichia coli. Nucleic Acids Res. *45*, 793-804.

Traxler, M.F., Summers, S.M., Nguyen, H.T., Zacharia, V.M., Hightower, G.A., Smith, J.T., and Conway, T. (2008). The global, ppGpp-mediated stringent response to amino acid starvation in Escherichia coli. Mol. Microbiol. *68*, 1128-1148.

Tuomanen, E., Cozens, R., Tosch, W., Zak, O., and Tomasz, A. (1986). The rate of killing of Escherichia coli by beta-lactam antibiotics is strictly proportional to the rate of bacterial growth. J Gen Microbiol *132*, 1297-1304.

Vallenet, D., Belda, E., Calteau, A., Cruveiller, S., Engelen, S., Lajus, A., Le Fevre, F., Longin, C., Mornico, D., Roche, D.*, et al.* (2013). MicroScope--an integrated microbial resource for the curation and comparative analysis of genomic and metabolic data. Nucleic Acids Res. *41*, D636-647.

Varik, V., Oliveira, S.R.A., Hauryliuk, V., and Tenson, T. (2017). HPLC-based quantification of bacterial housekeeping nucleotides and alarmone messengers ppGpp and pppGpp. Sci Rep *7*, 11022.

Wallace, A.C., Laskowski, R.A., and Thornton, J.M. (1995). LIGPLOT: a program to generate schematic diagrams of protein-ligand interactions. Protein Eng *8*, 127-134.

Wang, B., Dai, P., Ding, D., Del Rosario, A., Grant, R.A., Pentelute, B.L., and Laub, M.T. (2019). Affinity-based capture and identification of protein effectors of the growth regulator ppGpp. Nat. Chem. Biol. *15*, 141-150.

861 Zhang, Y., Agrebi, R., Bellows, L.E., Collet, J.F., Kaever, V., and Grundling, A. (2017). Evolutionary
862 Adaptation of the Essential tRNA Methyltransferase TrmD to the Signaling Molecule 3',5'-cAMP in
863 Bacteria. J. Biol. Chem. *292*, 313-327.

864 Zhang, Y., Zbornikova, E., Rejman, D., and Gerdes, K. (2018). Novel (p)ppGpp Binding and
865 Metabolizing Proteins of Escherichia coli. MBio *9*.
866

Figure 1

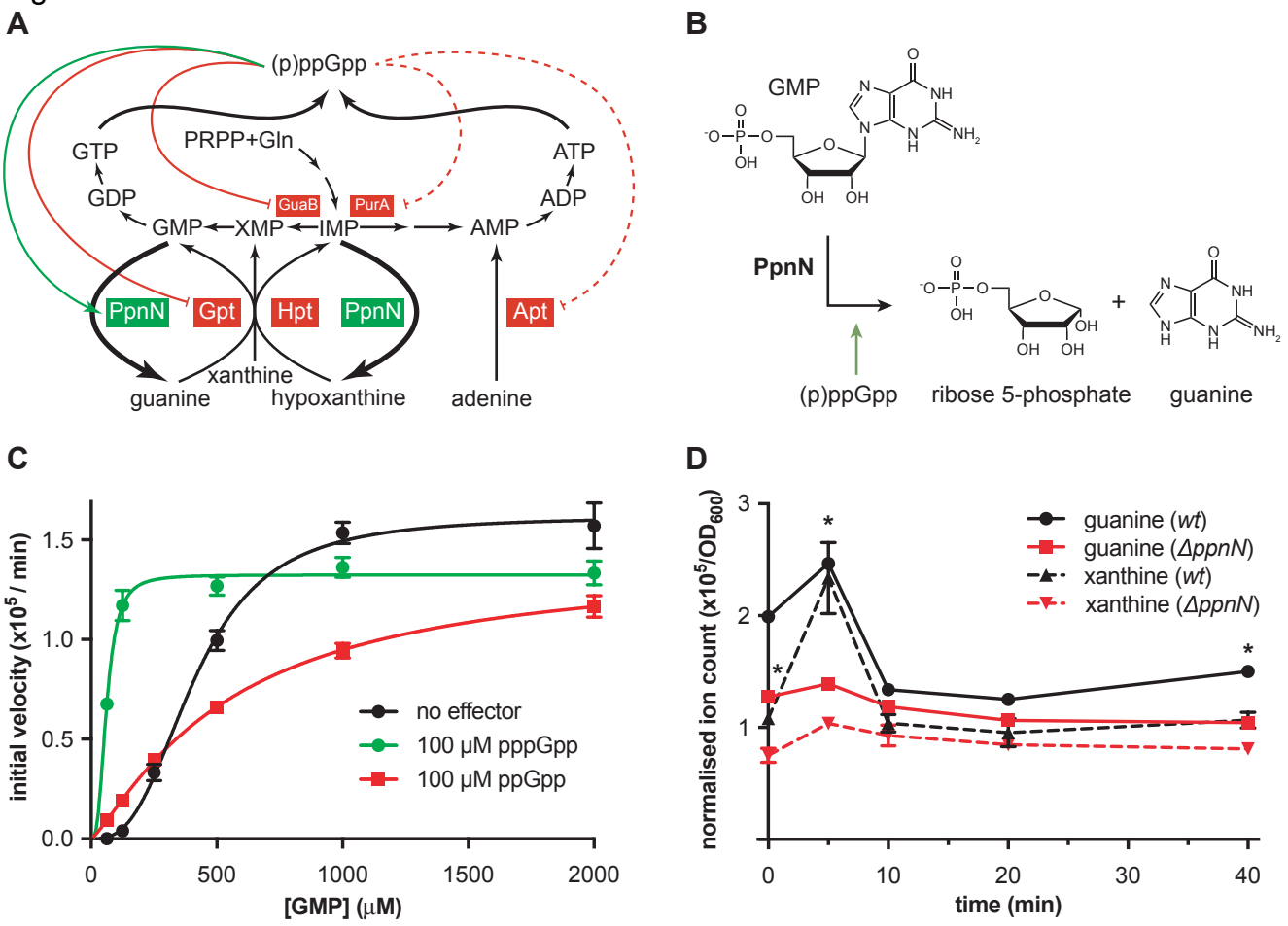
A
(p)ppGpp
GTP
PRPP+Gln
ATP
GDP
GuaB
PurA
ADP
GMP
XMP
IMP
AMP
PpnN
Gpt
Hpt
PpnN
Apt
xanthine
guanine
hypoxanthine
adenine
B
GMP
PpnN
(p)ppGpp
ribose 5-phosphate
guanine
C
initial velocity (x10^5 / min)
[GMP] (μM)
no effector
100 μM pppGpp
100 μM ppGpp
D
normalised ion count (x10^5/OD600)
time (min)
guanine (wt)
guanine (ΔppnN)
xanthine (wt)
xanthine (ΔppnN)

Figure 2

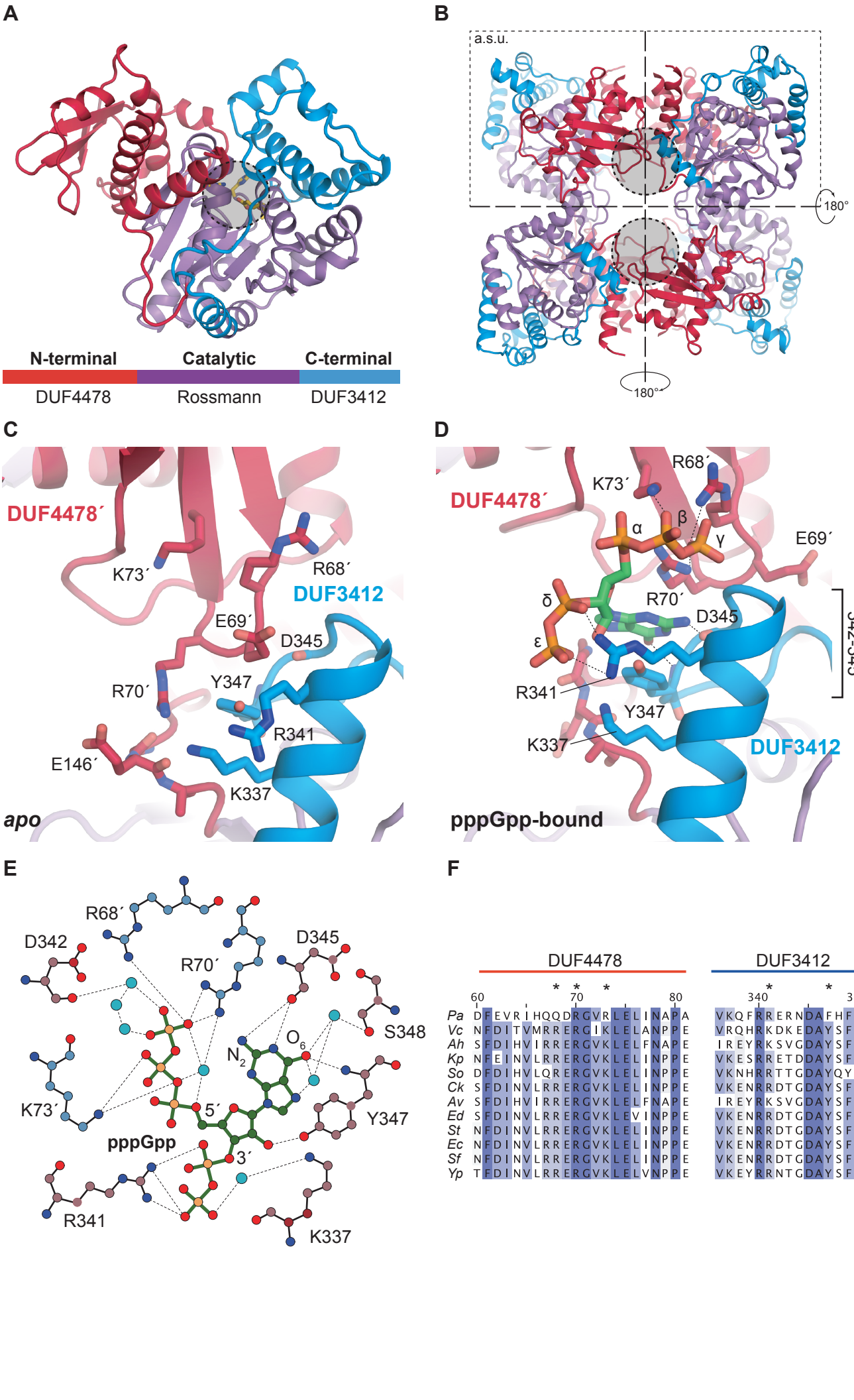
A
N-terminal
Catalytic
C-terminal
DUF4478
Rossmann
DUF3412
B
a.s.u.
180°
180°
C
DUF4478´
K73´
R68´
DUF3412
E69´
D345
R70´
Y347
R341
E146´
K337
apo
D
DUF4478´
K73´
R68´
α
β
γ
E69´
δ
R70´
D345
ε
342-345
R341
Y347
K337
DUF3412
pppGpp-bound
E
R68´
D342
D345
R70´
S348
O6
N2
K73´
5´
Y347
pppGpp
3´
R341
K337
F
DUF4478
DUF3412
60
70
80
340
350
Pa DFEVRIHQQDRGVRLELINAPA VKQFRRERNDAFHFNW
Vc NFDITVMRRERGIKLELANPPE VRQHRKDKEDAYSFNW
Ah SFDIHVIRRERGVKLELFNAPE IREYRKSVGDAYSFNW
Kp NFEINVLRRERGVKLELINPPE VKESRRETDDAYSFNW
So DFDIHVLQRERGVKLELINPPE VKNHRRTTGDAYQYQW
Ck SFDINVLRRERGVKLELINPPE VKENRRDTGDAYSFNW
Av SFDIHVIRRERGVKLELFNAPE IREYRKSVGDAYSFNW
Ed SFDINVLRRERGVKLEVINPPE VKENRRDTGDAYSFNW
St NFDINVLRRERGVKLELINPPE VKENRRDTGDAYSFNW
Ec NFDINVLRRERGVKLELINPPE VKENRRDTGDAYSFNW
Sf NFDINVLRRERGVKLELINPPE VKENRRDTGDAYSFNW
Yp TFDINVLRRERGVKLELVNPPE VKEYRRNTGDAYSFNW

Figure 3

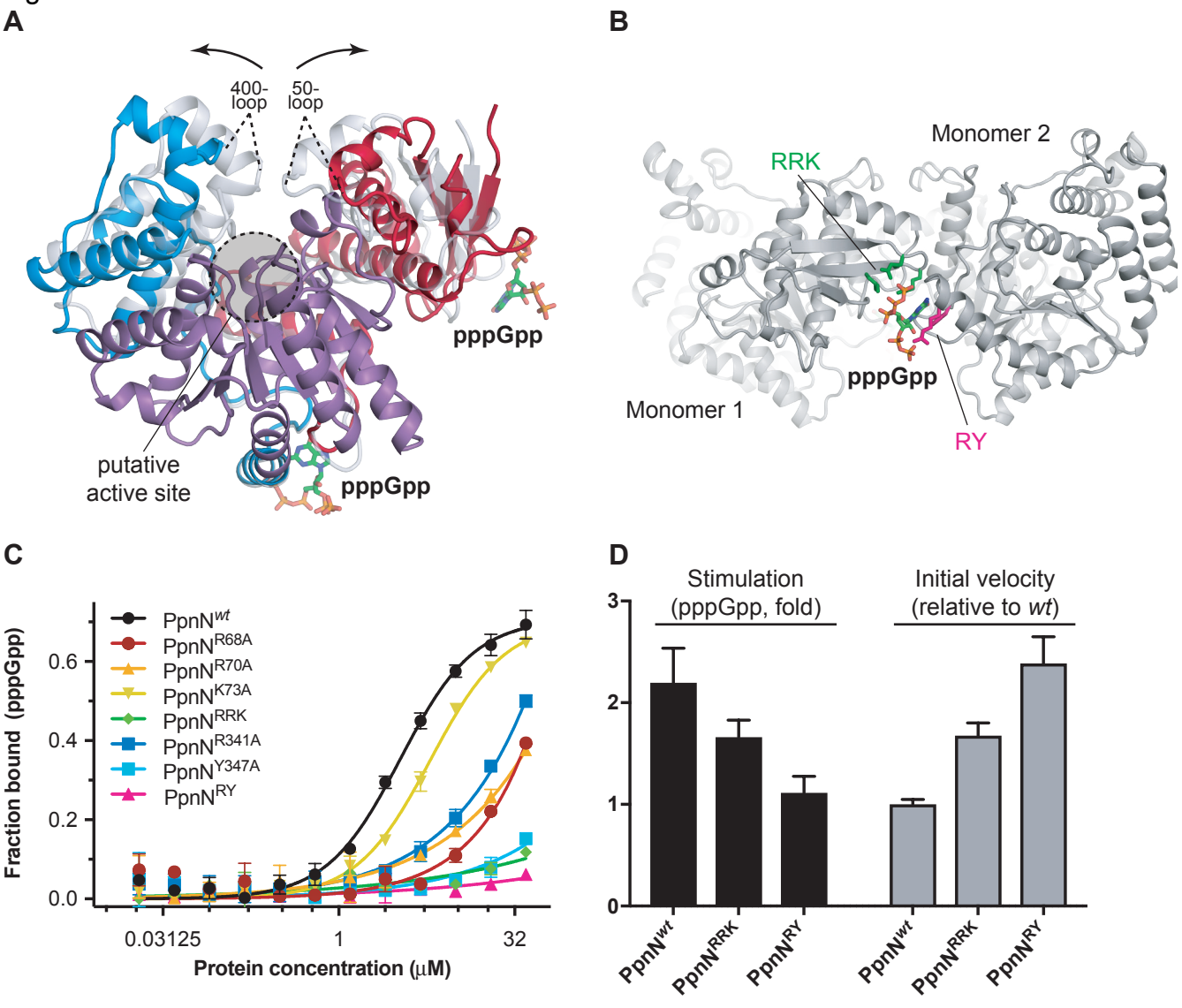
A
400-loop
50-loop
pppGpp
putative active site
pppGpp
B
Monomer 2
RRK
pppGpp
Monomer 1
RY
C
Fraction bound (pppGpp)
PpnN^wt
PpnN^R68A
PpnN^R70A
PpnN^K73A
PpnN^RRK
PpnN^R341A
PpnN^Y347A
PpnN^RY
0.0
0.2
0.4
0.6
0.03125
1
32
Protein concentration (μM)
D
Stimulation (pppGpp, fold)
Initial velocity (relative to wt)
0
1
2
3
PpnN^wt
PpnN^RRK
PpnN^RY
PpnN^wt
PpnN^RRK
PpnN^RY

Figure 4

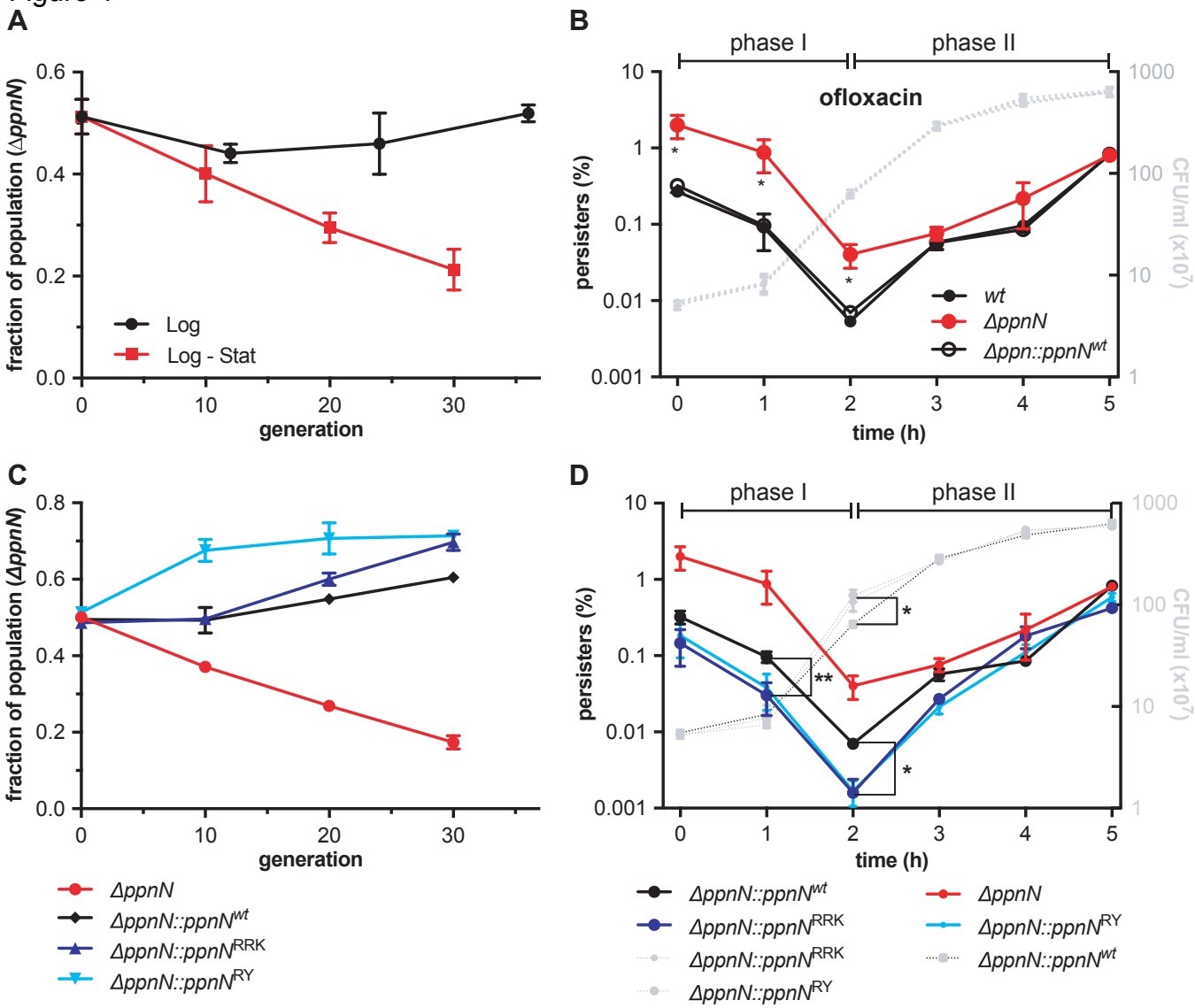
A
fraction of population (ΔppnN)
0.6
0.4
0.2
0.0
0
10
20
30
generation
Log
Log - Stat
B
phase I
phase II
ofloxacin
persisters (%)
10
1
0.1
0.01
0.001
CFU/ml (x10^7)
1000
100
10
1
0
1
2
3
4
5
time (h)
wt
ΔppnN
Δppn::ppnN^wt
C
fraction of population (ΔppnN)
0.8
0.6
0.4
0.2
0.0
0
10
20
30
generation
ΔppnN
ΔppnN::ppnN^wt
ΔppnN::ppnN^RRK
ΔppnN::ppnN^RY
D
phase I
phase II
persisters (%)
10
1
0.1
0.01
0.001
CFU/ml (x10^7)
1000
100
10
1
0
1
2
3
4
5
time (h)
**
*
*
ΔppnN::ppnN^wt
ΔppnN::ppnN^RRK
ΔppnN::ppnN^RRK
ΔppnN::ppnN^RY
ΔppnN
ΔppnN::ppnN^RY
ΔppnN::ppnN^wt

Figure 5

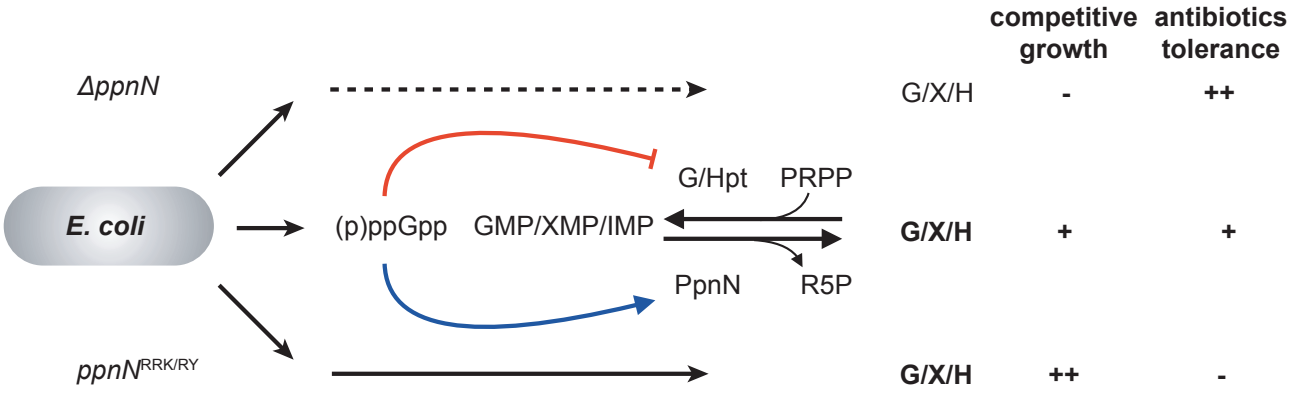
competitive growth
antibiotics tolerance
ΔppnN
G/X/H
-
++
E. coli
(p)ppGpp
GMP/XMP/IMP
G/Hpt
PRPP
PpnN
R5P
G/X/H
+
+
ppnN^RRK/RY
G/X/H
++
-

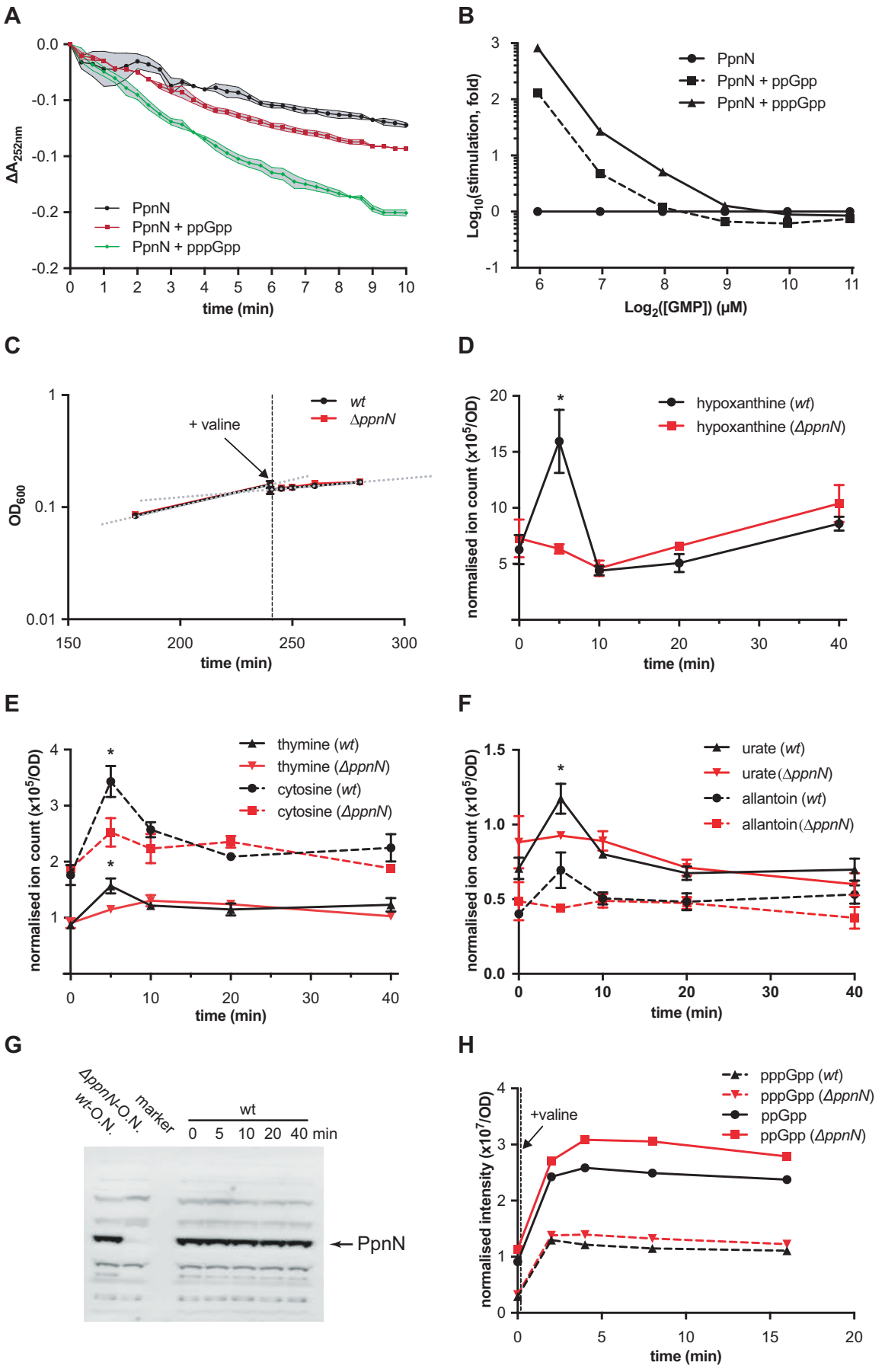
A
ΔA252nm
time (min)
PpnN
PpnN + ppGpp
PpnN + pppGpp
B
Log10(stimulation, fold)
Log2([GMP]) (μM)
PpnN
PpnN + ppGpp
PpnN + pppGpp
C
OD600
+ valine
wt
ΔppnN
time (min)
D
normalised ion count (x10^5/OD)
hypoxanthine (wt)
hypoxanthine (ΔppnN)
time (min)
E
normalised ion count (x10^5/OD)
thymine (wt)
thymine (ΔppnN)
cytosine (wt)
cytosine (ΔppnN)
time (min)
F
normalised ion count (x10^5/OD)
urate (wt)
urate (ΔppnN)
allantoin (wt)
allantoin (ΔppnN)
time (min)
G
ΔppnN-O.N.
wt-O.N.
marker
wt
0 5 10 20 40 min
PpnN
H
normalised intensity (x10^7/OD)
+valine
pppGpp (wt)
pppGpp (ΔppnN)
ppGpp
ppGpp (ΔppnN)
time (min)

Figure S1. (p)ppGpp stimulates PpnN to degrade purine nucleotides, Related to Figure 1. A. Degradation of XMP to xanthine by *E. coli* PpnN as measured spectroscopically at 252 nm, in the absence or presence of 100 μM pppGpp or ppGpp as indicated. Three replicates were performed for each reaction and the data are represented by mean ± SEM. **B.** Fold stimulation of PpnN activity calculated from the data in Figure 1C by normalisation of the respective initial reaction velocities in the absence or presence of 100 μM pppGpp or ppGpp (as indicated) to those of the *apo* enzyme at each GMP concentration. **C.** Growth curves of *wt* and Δ*ppnN E. coli* strains in MOPS medium before and after valine-induced isoleucine starvation (arrow). Linear regression of the slopes is indicated by the dashed, grey lines. **D.** Intracellular levels of hypoxanthine in *E. coli wt* and Δ*ppnN* strains grown in MOPS medium before (0 min) and after valine-induced isoleucine starvation as in **C**, measured by untargeted mass spectrometry. Three biological replicates were performed and the data are represented by mean ± SEM. **E.** Thymine and cytosine levels, as in **D**. **F.** Allantoin and urate levels, as in **D**. **G.** Western blot using anti-PpnN antiserum to probe *E. coli wt* and Δ*ppnN* cells grown in MOPS medium before (0 min) and after valine-induced isoleucine starvation as indicated. *wt*-O.N. and Δ*ppnN*-O.N. are from overnight cells of *wt* and Δ*ppnN* cells grown in MOPS medium, respectively. **H.** Levels of pppGpp and ppGpp measured by autoradiography in *E. coli wt* and Δ*ppnN* cells after by valine-induced isoleucine starvation. Intensities in arbitrary units were normalised by OD_{600}. Three biological replicates were performed and one representative experiment is shown.

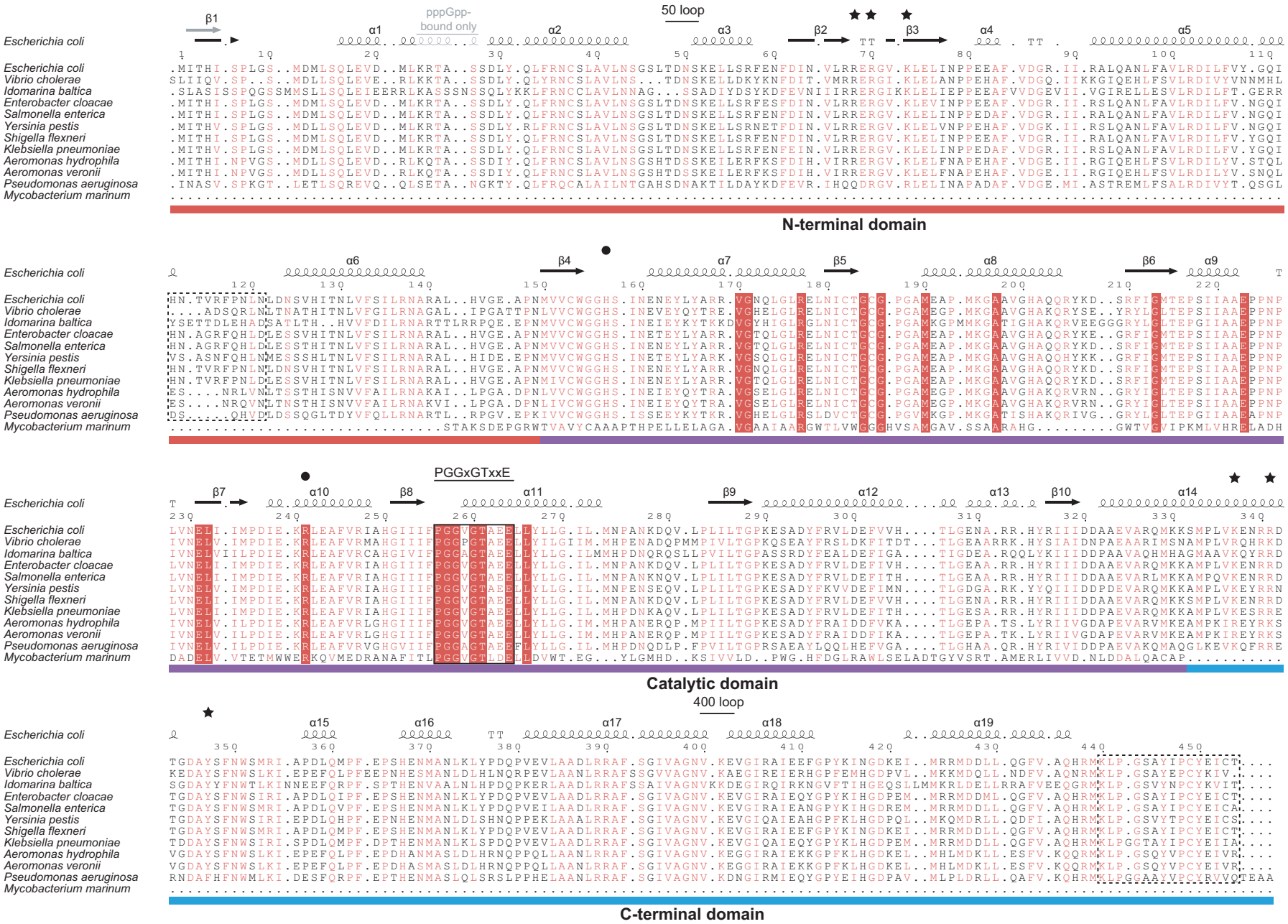
β1
α1
pppGpp-bound only
α2
50 loop
α3
β2
β3
α4
α5
Escherichia coli
Escherichia coli
Vibrio cholerae
Idomarina baltica
Enterobacter cloacae
Salmonella enterica
Yersinia pestis
Shigella flexneri
Klebsiella pneumoniae
Aeromonas hydrophila
Aeromonas veronii
Pseudomonas aeruginosa
Mycobacterium marinum
N-terminal domain
α6
β4
α7
β5
α8
β6
α9
Escherichia coli
Escherichia coli
Vibrio cholerae
Idomarina baltica
Enterobacter cloacae
Salmonella enterica
Yersinia pestis
Shigella flexneri
Klebsiella pneumoniae
Aeromonas hydrophila
Aeromonas veronii
Pseudomonas aeruginosa
Mycobacterium marinum
PGGxGTxxE
β7
α10
β8
α11
β9
α12
α13
β10
α14
Escherichia coli
Escherichia coli
Vibrio cholerae
Idomarina baltica
Enterobacter cloacae
Salmonella enterica
Yersinia pestis
Shigella flexneri
Klebsiella pneumoniae
Aeromonas hydrophila
Aeromonas veronii
Pseudomonas aeruginosa
Mycobacterium marinum
Catalytic domain
400 loop
α15
α16
α17
α18
α19
Escherichia coli
Escherichia coli
Vibrio cholerae
Idomarina baltica
Enterobacter cloacae
Salmonella enterica
Yersinia pestis
Shigella flexneri
Klebsiella pneumoniae
Aeromonas hydrophila
Aeromonas veronii
Pseudomonas aeruginosa
Mycobacterium marinum
C-terminal domain

Figure S2. Structure-guided sequence alignment of 12 representative PpnN homologues, Related to Figure 2. Amino acid sequences are shown for PpnN orthologues from a range of bacteria, including several pathogens, with the *E. coli* PpnN sequence at the top. Sequence numbers and secondary structure elements (top) and domain boundaries (bottom) correspond to the *E. coli* PpnN structure presented here. A small change of secondary structure in the N-terminus of PpnN on the pppGpp-bound form is shown in grey. The last sequence represents the sequence of a cytokinin riboside 5'-monophosphate phosphoribohydrolase from *M. marinum* with homology to the catalytic domain of PpnN (gene MMAR_4233, PDB ID 3SBX). TT is a β-turn. Residues involved in pppGpp binding are shown with stars (★) while putative active site residues are indicated with spheres (●). The conserved active site motif (PGGxGTxxE) and interacting loops (the 50 and 400 loops) are indicated as well. Dots indicate gaps in the alignment and dashed boxes regions which are disordered in the *apo* form. The C-terminus is disordered in both structures.

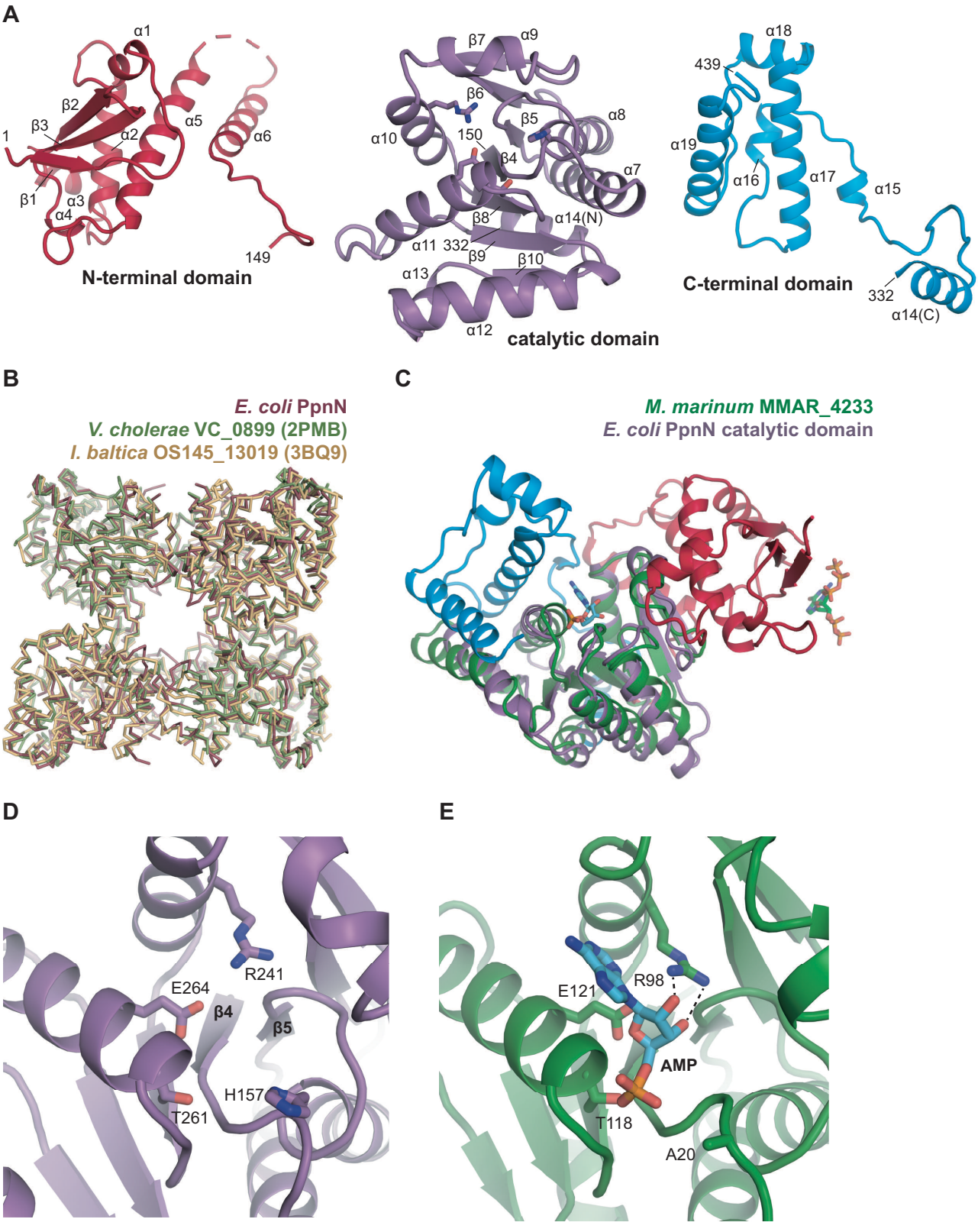
A
α1
β2
β3
1
α2
α5
α6
β1
α3
α4
149
N-terminal domain
β7
α9
β6
α8
α10
150
β5
β4
α7
β8
α14(N)
α11
332
β9
β10
α13
α12
catalytic domain
α18
439
α19
α16
α17
α15
C-terminal domain
332
α14(C)
B
E. coli PpnN
V. cholerae VC_0899 (2PMB)
I. baltica OS145_13019 (3BQ9)
C
M. marinum MMAR_4233
E. coli PpnN catalytic domain
D
R241
E264
β4
β5
H157
T261
E
E121
R98
AMP
T118
A20

Figure S3. Comparison of *E. coli* PpnN to its structural homologues and details of pppGpp binding, Related to Figure 2. A. Left, the N-terminal (DUF4478) domain of *E. coli* PpnN shown as cartoon with secondary structure elements and domain boundaries (1-149) indicated; middle, the catalytic (core) domain (150-332). Note that α14 has one half in the catalytic (central) domain and the other half in the C-terminal domain, which is based on sequence conservation; right, the C-terminal (DUF3412) domain (332-439). **B.** Alignment of the structure of *E. coli* PpnN (red) with its homologues from *Vibrio cholerae* (PDB ID 2PMB, green) and *Idomarina baltica* (PDB ID 3BQ9, yellow) (Bonanno et al., 2005). **C.** Structural overlay of the *E. coli* PpnN core (catalytic) domain (purple) with the structure of the catalytic domain from the *M. marinum* nucleotide-binding protein (PDB ID 3SBX, green) determined in complex with adenosine monophosphate (AMP) (Baugh et al., 2015). The PpnN N (red) and C (blue) terminal domains are also shown for reference. **D.** Close-up view of the predicted active site of *E. coli* PpnN with putative catalytic residues highlighted. **E.** Close-up of the active site region in the *M. marinum* structure in complex with adenosine monophosphate (AMP). Interacting active site residues are highlighted (Baugh et al., 2015).

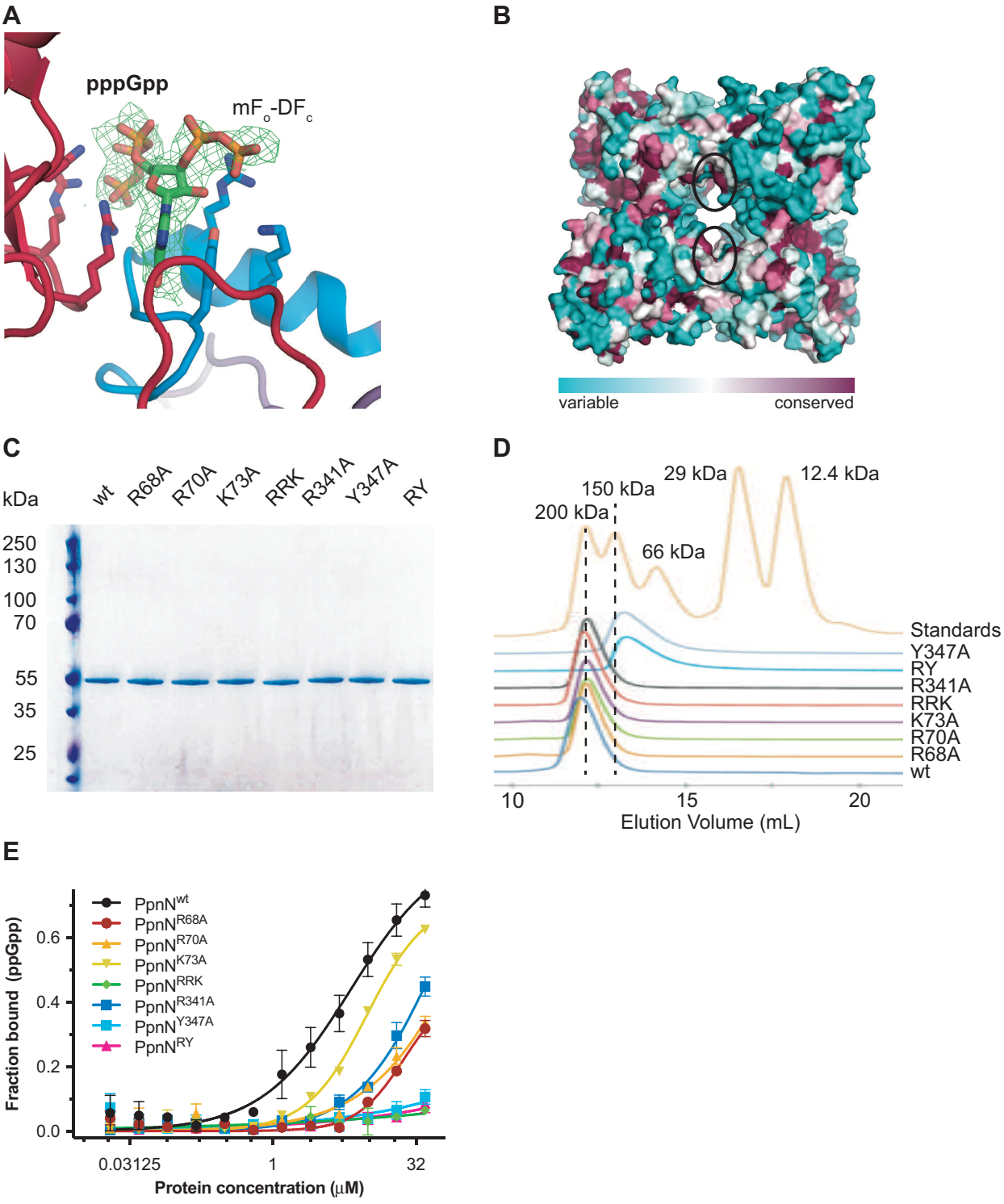

Figure S4. Mutational studies of PpnN, Related to Figure 3. A. The pppGpp binding site located between the N-terminal (red) and C-terminal (blue) domains of adjacent subunits of PpnN. pppGpp is shown as green/orange sticks along with unbiased, initial difference electron density (mF$_o$-DF$_c$)

contoured at 2.0σ. **B.** Conservation of PpnN sequences mapped onto the structure using ConSurf (Landau et al., 2005) with the binding sites of pppGpp circled (two sites per circle). The scale bar indicates the level of conservation from variable (cyan) to conserved (burgundy). **C.** SDS-PAGE of purified *E. coli wt* and mutant PpnN proteins (1 μg each). **D.** Size exclusion chromatography of approximately equal amounts of purified *E. coli wt* and mutant PpnN proteins, alongside protein standards as indicated. **E.** DRaCALA binding curves of α-^{32}P-ppGpp using *E. coli wt* and mutant PpnN proteins. The curves were fit using a non-linear one-site total binding model in GraphPad Prism. At least three replicates were performed for each reaction, and the data are represented by mean ± SEM.

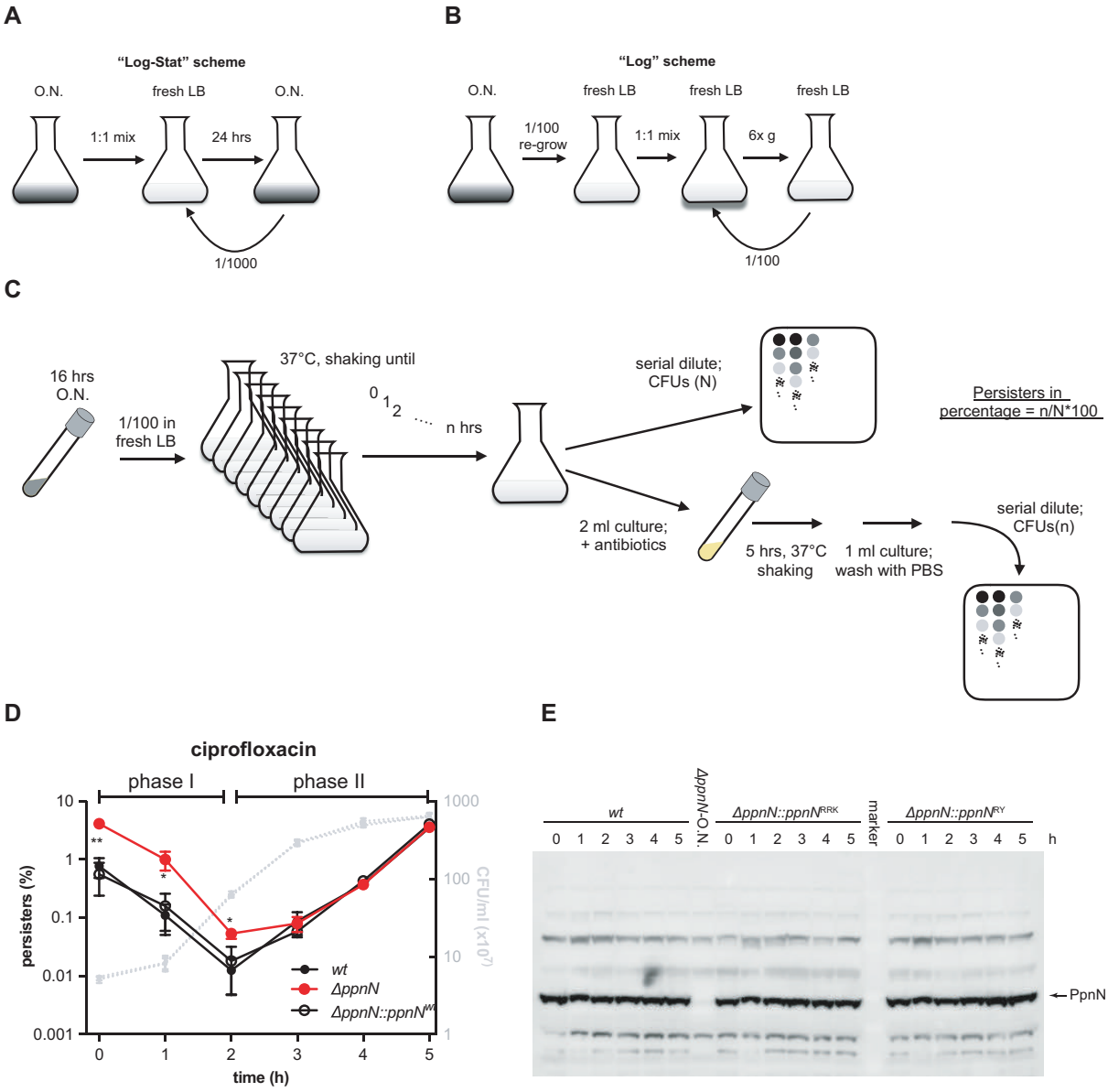

Figure S5. Analysis of *E. coli* fitness and persistence levels, Related to Figure 4. A. Overview of the "Log-Stat" scheme of competitive growth: Overnight (O.N.) cells of two tested strains were mixed 1:1 into fresh LB-B broth starting from OD_{600}=0.005. 24 h later, the mixed O.N. culture was sub-cultured in fresh LB-B broth, again starting from OD_{600}=0.005. This process was repeated. The fraction of each strain in the population was determined after every 24 h on LB agar plates. **B.** Overview of the "Log" scheme of competitive growth: Overnight (O.N.) cells of two tested strains were first sub-cultured in fresh LB-B broth and grown to log phase, when a 1:1 mixture of both strains

was inoculated into fresh LB-B broth starting from OD_{600}=0.005. About 2 h (6 generations) later, the mixed culture was sub-cultured in fresh LB-B broth, again starting from OD_{600}=0.005. This process was repeated. The fraction of each strain in the population was determined after every 12 generations on LB agar plates. **C.** Experimental setup for the persistence assay (see STAR Methods for details) **D.** Colony-forming units (CFUs, $x10^7$/ml, in grey) and ciprofloxacin (10 μg/ml) killing assay (persistence) for *E. coli wt*, Δ*ppnN*, and the *in situ* complemented strain Δ*ppnN::ppnN*^{wt} during growth resumption in LB-B broth from 16 hrs overnight cultures. The data are represented by mean ± SEM. **E.** Western blot probing PpnN protein from *E. coli wt*, Δ*ppnN::ppnN*^{RRK} and Δ*ppnN::ppnN*^{RY} strains during growth resumption from 16 hrs overnight cultures in fresh LB-B broth. Δ*ppnN*-O.N. is overnight cells of Δ*ppnN* strain in LB-B media.

SUPPLEMENTARY TABLES

Table S1. Bacterial strains used in this study, Related to Figure 1.

Strain	**Relevant features**	**Reference**
DH5α	Cloning strain	Stratagene
BL21(DE3)	*E. coli* strain used for protein expression	Novagen
YZ37	MG1655	Laboratory stock
YZ281	MG1655 *lacZ::kan*	This study
YZ365	MG1655 *ΔppnN lacZ::kan*	This study
YZ&6	DH5α pCA24N-PpnN(wt); CamR	(Kitagawa et al., 2005)
YZ293	DH5α pCA24N-PpnN(R68A); CamR	This study
YZ294	DH5α pCA24N-PpnN(R70A); CamR	This study
YZ295	DH5α pCA24N-PpnN(K73A); CamR	This study
YZ296	DH5α pCA24N-PpnN(R68AR70AK73A); CamR	This study
YZ297	DH5α pCA24N-PpnN(R341A); CamR	This study
YZ298	DH5α pCA24N-PpnN(Y347A); CamR	This study
YZ299	DH5α pCA24N-PpnN(R341AY347A); CamR	This study
YZ300	BL21 DE3 pCA24N-PpnN(R68A); CamR	This study
YZ301	BL21 DE3 pCA24N-PpnN(R70A); CamR	This study
YZ302	BL21 DE3 pCA24N-PpnN(K73A); CamR	This study
YZ303	BL21 DE3 pCA24N-PpnN(R68AR70AK73A); CamR	This study
YZ304	BL21 DE3 pCA24N-PpnN(R341A); CamR	This study
YZ305	BL21 DE3 pCA24N-PpnN(Y347A); CamR	This study
YZ306	BL21 DE3 pCA24N-PpnN(R341AY347A); CamR	This study
YZ309	MG1655 pWRG99; Amp	This study
YZ310	DH5α pWRG100; Amp, Cam	This study
YZ340	MG1655 pWRG99 *ppnN::SceI-cam*; Amp; Cam	This study
YZ362	MG1655 *ΔppnN* pWRG99; Amp	This study
YZ364	MG1655 *ΔppnN*	This study
YZ366	MG1655 *ΔppnN::SceI-cam* pWRG99; Amp; Cam	This study
YZ368	MG1655 Δ*ppnN::ppnN*^{wt}*;* pWRG99; Amp	This study
YZ370	MG1655 Δ*ppnN::ppnN*^{wt}	This study
YZ372	MG1655 Δ*ppnN::ppnN*^{RRK}*;* pWRG99; Amp	This study
YZ374	MG1655 Δ*ppnN::ppnN*^{RY}*;* pWRG99; Amp	This study
YZ378	MG1655 Δ*ppnN::ppnN*^{RRK}	This study
YZ380	MG1655 Δ*ppnN::ppnN*^{RY}	This study

Table S2. Primers used in this study, Related to Figure 3.

Number	Name	Sequence
PYZ34	pCA24Nf	GGCCCTTTCGTCTTCACCTC
PYZ35	pCA24Nr	GGCAACCGAGCGTTCTGAAC
PYZ212	DygdH-conf-F	ATCGACCACAAGACTGGTTC
PYZ213	DygdH-conf-R	GAAAATAGGGAAACGTTTGC
PYZ248	QCygdH(R68A)-F	GTCTTGCGCGCTGAACGCGGCGTAAA
PYZ249	QCygdH(R68A)-R	CGCGTTCAGCGCGCAAGACGTTAATATCG
PYZ250	QCygdH(R70A)-F	GCCGTGAAGCCGGCGTAAAGCTGGAAC
PYZ251	QCygdH(R70A)-R	TTACGCCGGCTTCACGGCGCAAGAC
PYZ252	QCygdH(K73A)-F	GCGGCGTAGCGCTGGAACTGATTAATCCCC
PYZ253	QCygdH(K73A)-R	GTTCCAGCGCTACGCCGCGTTCACG
PYZ254	QCygdH(R68R70K73AAA)-F	TTGCGCGCTGAAGCCGGCGTAGCGCTGGAACTGATTAATCCCC
PYZ255	QCygdH(R68R70K73AAA)-R	TTCCAGCGCTACGCCGGCTTCAGCGCGCAAGACGTTAATATCG
PYZ256	QCygdH(R341A)-F	GAAAATCGCGCTGATACAGGCGATGCCTAC
PYZ257	QCygdH(R341A)-R	CTGTATCAGCGCGATTTTCTTTCACCAGC
PYZ258	QCygdH(Y347A)-F	GCGATGCCGCCAGCTTTAACTGGTCAATGC
PYZ259	QCygdH(Y347A)-R	TAAAGCTGGCGGCATCGCCTGTATCAC
PYZ260	QCygdH(R341Y347A)-F	CGCGCTGATACAGGCGATGCCGCCAGCTTTAACTGGTCAATGC
PYZ261	QCygdH(R341Y347A)-R	TGGCGGCATCGCCTGTATCAGCGCGATTTTCTTTCACCAGC
PYZ273	SceI-ygdH29-F	TATTAGCCCGCTTGGCTCCATGGATATGTTGTCGCAGCTGCTAGACTATATTACCCT GTTATCCC
PYZ274	SceI-ygdH29-R	TAGAGGTCGCTGCTGGCGGTGCGTTTAAGCATATCCACTTATTTAAATGGCGCGCCT TAC
PYZ285	SceI-ygdHCt-R	GAAAACCCGGCAACAAACGTCACCGGGGGAGCGGAGATTAATTTAAATGGCGCGCC TTAC
PYZ283	80mer-ygdH-Ifdel-F	TATTAGCCCGCTTGGCTCCATGGATATGTTGTCGCAGCTGTAATCTCCGCTCCCCCG GTGACGTTTGTTGCCGGGTTTTC
PYZ284	80mer-ygdH-Ifdel-R	GAAAACCCGGCAACAAACGTCACCGGGGGAGCGGAGATTACAGCTGCGACAACATA TCCATGGAGCCAAGCGGGCTAATA